



**HAL**  
open science

# Efficiency of EB CFRP composites for flexural strengthening of continuous RC beams: A comparative study with NSM CFRP rods

Mohammad Abdallah, Firas Al-Mahmoud, Abdelouahab Khelil, Julien Mercier

## ► To cite this version:

Mohammad Abdallah, Firas Al-Mahmoud, Abdelouahab Khelil, Julien Mercier. Efficiency of EB CFRP composites for flexural strengthening of continuous RC beams: A comparative study with NSM CFRP rods. Structures, 2021, 34, pp.1567-1588. 10.1016/j.istruc.2021.08.073 . hal-03976004

**HAL Id: hal-03976004**

**<https://hal.science/hal-03976004>**

Submitted on 16 Oct 2023

**HAL** is a multi-disciplinary open access archive for the deposit and dissemination of scientific research documents, whether they are published or not. The documents may come from teaching and research institutions in France or abroad, or from public or private research centers.

L'archive ouverte pluridisciplinaire **HAL**, est destinée au dépôt et à la diffusion de documents scientifiques de niveau recherche, publiés ou non, émanant des établissements d'enseignement et de recherche français ou étrangers, des laboratoires publics ou privés.



Distributed under a Creative Commons Attribution - NonCommercial 4.0 International License

## Efficiency of EB CFRP composites for flexural strengthening of continuous RC beams: A comparative study with NSM CFRP rods

Mohammad Abdallah\*<sup>1</sup>, Firas Al Mahmoud<sup>1</sup>, Abdelouahab Khelil<sup>1</sup> and Julien Mercier<sup>2</sup>

<sup>1</sup>*Institut Jean Lamour, UMR 7198, CNRS, Université de Lorraine, Nancy, France*

<sup>2</sup>*Freyssinet, Paris, France*

\*corresponding author: Mohammad Abdallah, E-mail [mohammad.abdallah@univ-lorraine.fr](mailto:mohammad.abdallah@univ-lorraine.fr)

**Abstract:** ~~During the last few decades, carbon fiber reinforced polymer (CFRP) composites have become popular in the construction industry. These composites are normally applied to structural members to improve their carrying capacity and extend their service life. The techniques most commonly used for this purpose are external bonding (EB) and near surface mounting (NSM). These techniques are continuously investigated to verify or to improve their efficiency. However, statically indeterminate reinforced concrete (RC) members such as continuous beams are the most widely used structural form. Although most *in situ* RC beams are indeterminate constructions, application of the EB and NSM techniques remains confined to simply supported beams, in which CFRP composites are applied in the sagging moment region. The flexural behavior and failure modes of multispan beams are considerably different from those of simply supported ones. Therefore,~~ This paper presents an experimental study of the use of carbon fiber-reinforced polymer (CFRP) composites to strengthen two-span reinforced concrete (RC) beams. ~~First,~~ Six large-scale beams were strengthened in hogging and sagging regions according to the external bonding (EB) technique and then statically tested to investigate the impact of the CFRP position (~~side, top/bottom~~), CFRP form (~~sheet, plate~~), CFRP layers (~~one layer, multiple layers~~), and weight of carbon fibers ~~per unit area (350 g/m<sup>2</sup>, 700 g/m<sup>2</sup>)~~ on the flexural performance of continuous beams. The experimental results of the strengthened beams were carefully studied in terms of load-carrying capacity, failure modes, cracking patterns, moment redistribution, and reinforcement strain and compared with the results of an unstrengthened control beam. The efficiency of the EB technique in strengthening continuous RC beams was assessed through a comparative study with the near surface mounted (NSM) technique. For this purpose, another two beam specimens strengthened with NSM-CFRP bars were considered. Based on the experimental results, a general improvement in the flexural performance of strengthened beams was observed. By applying the EB-CFRP composites, the yield and ultimate load capacity could be improved up to 59.1% and 49.8% respectively. ~~The results showed that the side bonding system is a convenient alternative to the conventional one for strengthening beams. Moreover,~~ The results also showed that increasing the carbon fiber weight was found to be effective in improving the strength capacity of beams and it may use as an alternative to multiple sheet layers., ~~but this efficiency was conditional upon the total axial stiffness ratio of the beam and uses a proper adhesive epoxy resin. Furthermore, The moment redistribution that was~~

~~found to occur in the stage between the concrete cracking and the first steel yielding cannot be neglected and should be used when calculating the redistribution degree of EB CFRP members. Second, an evaluation of the effectiveness of current analytical provisions in determining the flexural strength of EB CFRP continuous beams was conducted. The assessments showed that the American and Italian guidelines are (relatively) more appropriate than the FIB Bulletin 14 guideline. However, they accurately predicted the ultimate strength of beams strengthened with one CFRP layer, but not with multiple layers. Third, The efficiency of the EB technique in strengthening continuous RC beams was assessed through a comparative study with the near surface mounted (NSM) technique. For this purpose, another two beam specimens strengthened with NSM CFRP bars were considered. the results obtained from testing another two beam specimens strengthened internally with NSM CFRP bars were presented and analyzed. Comparisons regarding the global flexural performance, including failure modes and load-carrying capacities, allow confirming the higher efficiency of the NSM system in comparison to the EB one.~~

**Keywords:** EB; NSM; strengthening; continuous RC beam; comparison.

## 1. Introduction

Fiber-reinforced polymers (FRPs) are increasingly being used in the field of civil engineering due to their mechanical strengthening advantages. Among the various composite materials available, carbon fiber-reinforced polymers (CFRPs) are considered the most used and are widely preferable. In general, CFRPs have a high tensile strength and modulus of elasticity and exhibit excellent resistance to corrosion and creep rupture [1]. CFRP materials in the form of plates or sheets can be applied to damaged structural elements as an external reinforcement via the external bonding (EB) technique [2], whereas those in the form of rods are used as an internal reinforcement via the near surface mounted (NSM) technique [3]. Generally, the efficiency of the CFRPs used in reinforced concrete (RC) structures depends on their interface bonding behavior with concrete, which can normally be achieved using an epoxy-resin agent. Such bonding behavior is essentially affected by the mechanical properties of the CFRP and the adhesive epoxy-resin materials, as well as the roughness of the concrete surface [4, 5]. ~~With regard to~~ Regarding the latter, both ~~of~~ the EB and NSM techniques have different construction processes, implying different bond strength levels.

Although CFRP materials were used for the first time more than 50 years ago to strengthen RC members, only a ~~very~~ limited number of research studies have investigated the use of such materials to strengthen statically indeterminate members, such as continuous beams [6-9]. Extensive research studies have been performed on the use of CFRPs to reinforce and retrofit simply supported beams (SSBs) [10-16], joints [17-19], and columns [20-22]. It has been found that the flexural strength improvement in SSBs as a result of CFRPs is significant and may reach, in some strengthening configurations, more than 90% with the EB technique [10] and even more than 130% with the NSM technique [23]. However, regardless of the strengthening technique

that is used, an essential drawback that has been reported is the nonconventional failure mode of the SSBs due to delamination and/or the tensile rupture of the EB-CFRP sheets/plates or pull-out of the NSM-CFRP rods. Under certain circumstances, such a nonconventional failure mode may occur at an early load stage in the form of concrete cover separation [24] or peeling-off failure [25], either of which can prevent the desired flexural strength enhancement in the beam. ~~A number of~~ Several end anchorage systems have been suggested to prevent such a premature failure in EB-CFRP sheet beams, such as U-strap [26], L-shaped jackets [27], and CFRP splay anchors [28], as well as in NSM-CFRP rod beams, such as end-steel plates [29]. ~~Some of these systems, however, are not convenient to implement in current constructions and may require a prior manufacturing process.~~ In contrast, the ACI 440.2R guideline [30] recommends that, on the one hand, FRP laminates should be terminated at least at a distance equal to the development length ( $l_{df}$ ) past the point along the span corresponding to the cracking moment ( $M_{cr}$ ) in the SSBs. In continuous beams, on the other hand, FRP laminates should be terminated at  $d/2$  or at least 150 mm beyond the inflection point (point of zero moment), where  $d$  is the cross-sectional effective depth.

A general review of the literature on strengthening SSBs using the EB and NSM techniques confirms their potential to enhance the flexural behavior of RC beams. However, their initial forms might not be feasible for some practical applications. These systems have several shortcomings due to the imposed architectural constraints, the insufficient dimensions of the beam itself, and the possibility of damaging other members, such as columns, during preparation and installation. Consequently, side-bonded CFRP sheets [10] and side-NSM-CFRP rods [11,23] have recently been proposed as convenient alternatives, although their effectiveness has not yet been investigated in continuous RC beams. Bilotta et al. [24] discussed the efficiency of the NSM and EB techniques in strengthening SSBs using CFRP strips and plates. The test results indicated that the NSM system is more effective than the EB system in improving the flexural strength although it is less effective in increasing the beam stiffness. Furthermore, NSM strips were found to be weakly sensitive to debonding phenomena. By contrast, Yihua Zeng et al [31] indicated that the strengthening technique type had a slight influence on the flexural performance of SSBs. Based on the experimental results, the RC beams strengthened with EB CFRP sheets and NSM FRP bars were found to have a very similar load-carrying capacity and failure mode (CFRP sheets or bars debonding and concrete crushing). To the best of our knowledge, there are no published studies comparing the efficiency of the EB and NSM systems in terms of strengthening continuous RC beams.

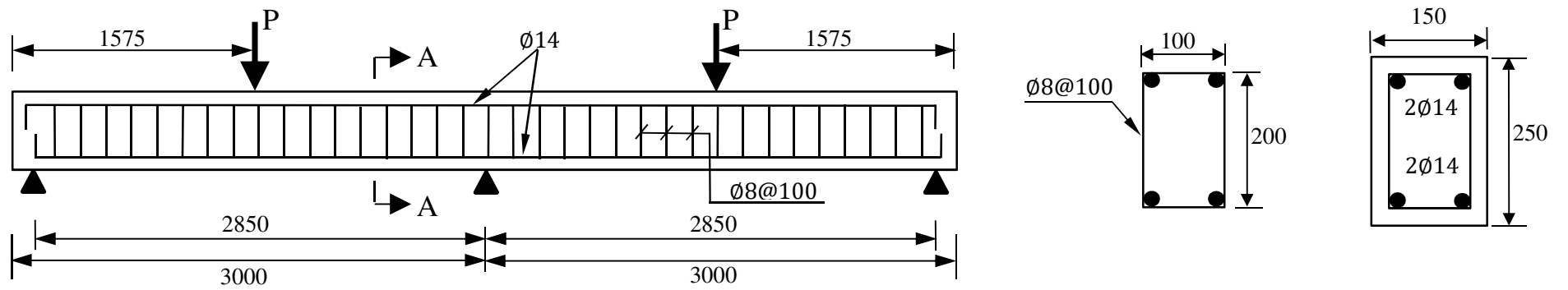
Unlike SSBs, continuous beams have positive (sagging) and negative (hogging) bending moment regions. Therefore, their flexural behavior and failure modes are considerably different from those of SSBs and are strongly associated with the strengthening arrangement of CFRP reinforcements. Ashour et al. [6] performed a series of experimental tests to study the performance of continuous two-span RC beams strengthened in flexure with EB-CFRP sheets. The test results showed that strengthening both the sagging and hogging regions is the most effective arrangement to enhance the beams' load-carrying capacity. The tested strengthened

specimens exhibited about 25% improvement in the ultimate load compared to their unstrengthened counterparts, and they failed because of the tensile rupture of the CFRP sheets, CFRP sheet separation, and brittle peeling failure of the concrete cover. The same strengthening arrangement was adopted by Akbarzadeh et al. [7] to experimentally study the influence of multilayer CFRP sheets on the flexural response of reinforced high-strength two-span beams. The authors found that increasing the number of layers can change the failure mode from tensile rupture to intermediate crack (IC) debonding of the CFRP sheets. The beam strengthened with three layers of CFRP sheets exhibited about 60% improvement in the load-carrying capacity compared to the control beam. Ali et al. [8] examined the flexural capacity and failure modes of continuous RC beams with three spans externally strengthened in the positive and negative moment regions with different lengths and layers of CFRP sheets. They concluded that the ultimate load of the strengthened beams increased by 16.7%–26.6% with respect to the control beam. The main failure modes observed were peeling-off and rupture of the CFRP sheets. Abdallah et al. [9] clarified that the contribution of NSM-CFRP rods to the improvement of the load-carrying capacity of statically indeterminate two-span RC beams is limited by the debonding of the CFRP bars in the negative bending moment zone or peeling-off of the concrete cover. Notably, the peeling-off failure occurred due to the insufficient CFRP rod length. However, the beam specimens were strengthened in both the hogging and sagging regions, and the improvement achieved in their load-carrying capacity ranged between 42% and 63% compared to the load-carrying capacity of the control beam. Abdzaid and Kamonna [32] experimentally investigated the flexural behavior of eleven continuous RC beams strengthened by NSM steel bars with different development lengths, diameters, and material types, with end-anchors of CFRP fabrics. The experimental results showed that the strengthened beams achieved a significant enhancement in ultimate flexural strength by approximately 108% relative to the control beam, and the CFRP end-anchorage can eliminate the separation of the concrete cover and demonstrates a significant improvement in ductility.

Moment redistribution is a key feature of continuous RC beams. In ordinary indeterminate beams, moment redistribution primarily depends on the amount of tension steel reinforcement ( $\rho_s$ ) in the critical sections. Indeed, at the ultimate state, moment transfer occurs from the hogging region to the sagging region when  $\rho_s^h/\rho_s^s$  is not greater than 1.0, whereas when  $\rho_s^h/\rho_s^s$  is greater than 1.5, moment transfer occurs from the sagging region to the hogging region. When  $\rho_s^h/\rho_s^s$  falls between 1.0 and 1.5, the moment transfer is indistinct [33]. Despite being very limited, previous experimental studies on strengthening RC beams with CFRP composites have indicated that moment redistribution in such members is possible to some extent at the ultimate state [7,9]. Nevertheless, moment redistribution not only occurs at the ultimate state but also evolves through the whole loading process, even before formation yielding of the tension steel reinforcement [33-34,35]. Indeed, Diab et al [35] found that the moment redistribution achieved after the beam cracking load until the failure load varies in accordance with the NSM strengthening region and the NSM strengthening material (steel or CFRP). On the other hand, Abdallah et al [36] found that the moment redistribution degree achieved in the ultimate state of

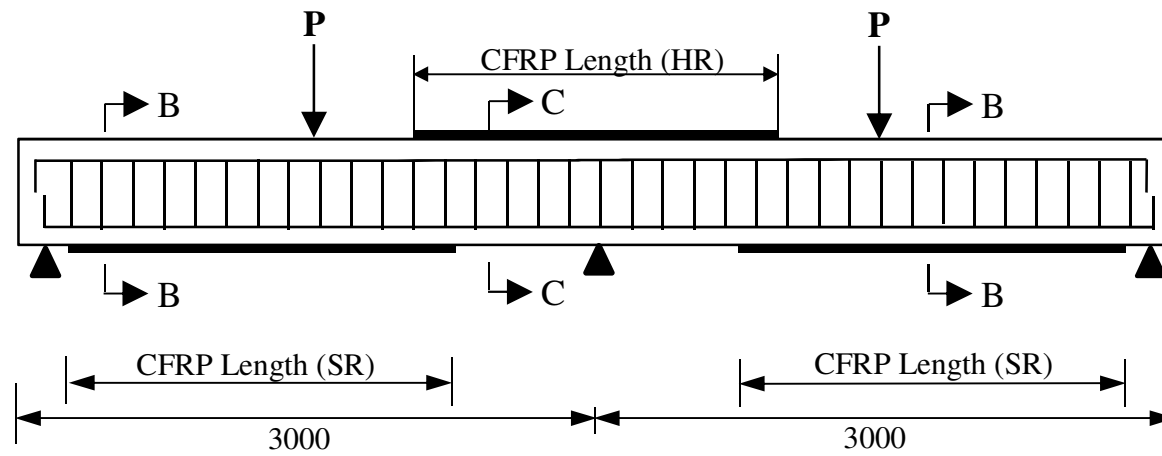
NSM strengthened beams is significantly affected by the position and arrangement of the CFRP bars.

As stated above, relatively few studies have been performed on continuous RC beams strengthened with either EB-CFRP or NSM-CFRP. Most of these studies have focused on the impact of the arrangement, number of layers, and length of CFRPs on the failure modes and flexural capacity of beams. It is worth mentioning that increasing the carbon fiber weight per unit area has recently been used in the construction and rehabilitation industry as an alternative to multiple sheet layers. However, there are no available studies in the literature exploring the effectiveness of that alternative in terms of improving the performance of continuous RC beams. Therefore, the primary aim of this study is to fill in the gaps in the literature regarding strengthening continuous RC beams with EB-CFRP. Generally, this study consists of three main sections. In the first section, seven large-scale two-span beams are statically investigated: one control beam and six beams initially strengthened in terms of bending with CFRP sheets or plates. The principle aim of the first section is to investigate the effects of important influential factors, such as (i) the CFRP reinforcement position; (ii) the CFRP form, either sheet or plate; (iii) the CFRP layer number; and (iv) the weight of the carbon fibers, on the load-carrying capacity, failure modes, cracking patterns, moment redistribution, and strain analysis of continuous beams. Because the current design guidelines have been developed to strengthen SSBs with EB-FRP laminates, the second part of this study evaluates the effectiveness of the current design codes in determining the flexural strength of continuous beams strengthened externally with CFRP sheets or plates. The experimental flexural strength capacities of the tested beams are compared with those obtained from the design formulas provided in the American ACI 440.2R-08 [30], the Italian CNR-DT 200 R1/2013 [37], and the technical report of ~~FIB~~ *fib* Bulletin 14 [38]. Finally, the third section assesses and compares the efficiencies of the EB and the NSM techniques. For this purpose, another two beams strengthened by means of the NSM and side-NSM-CFRP bars technique are tested and presented.

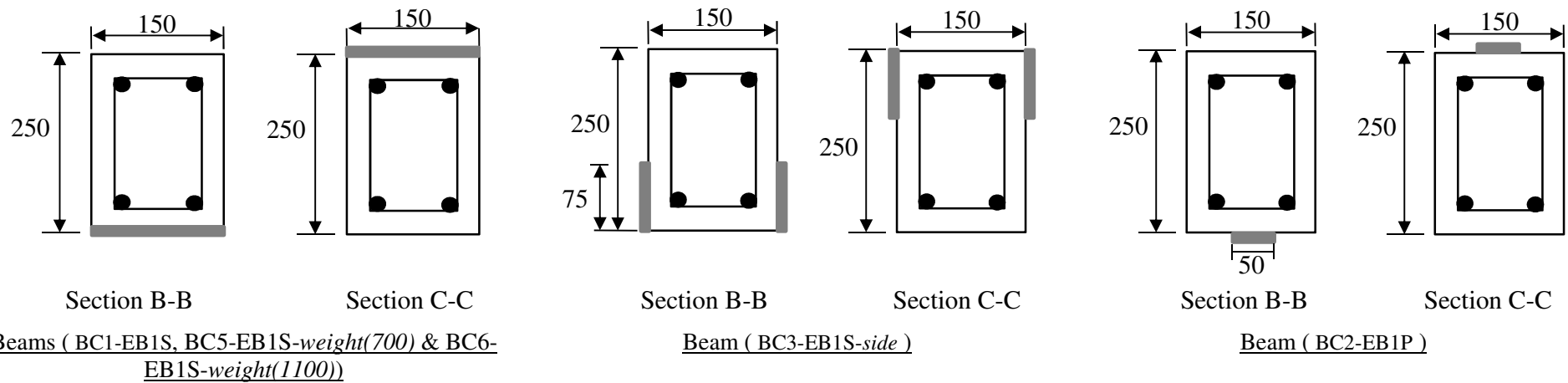


Section A-A

Fig. 1: Dimensions, steel reinforcement layout and support arrangement of the tested beams.



(a)





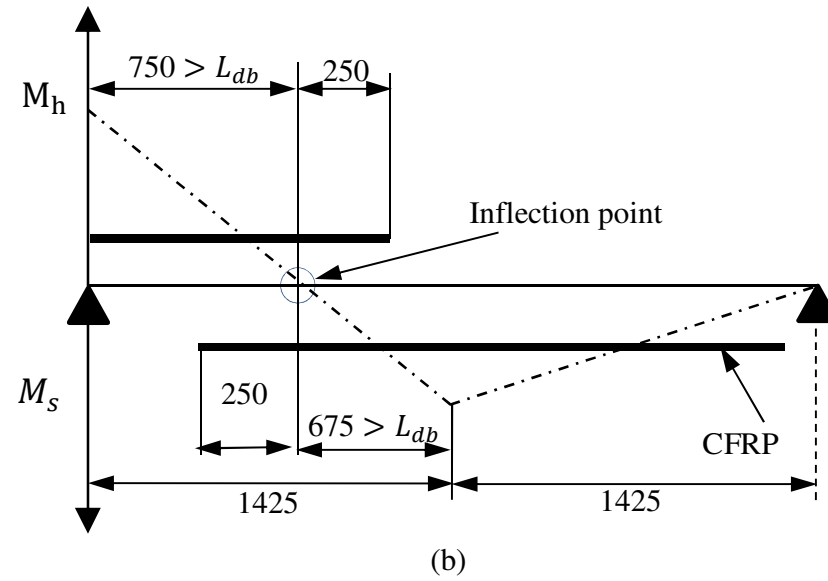
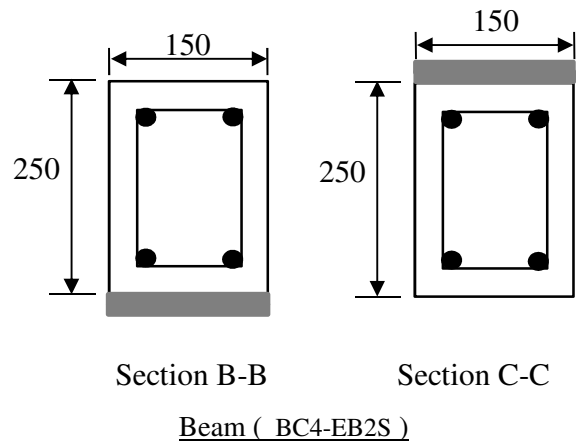


Fig. 2 : (a) Elevation view and cross-sections of the beam specimens and (b) Length of CFRP sheets/plates in beams. (All dimensions are in mm)

## 2. Experimental Program

### 2.1. Tested beams and material properties

#### 2.1.1 Beams strengthened with EB CFRP reinforcements

The test matrix in this section consists of seven full-scale two-span RC beams: one considered as a reference beam and six externally strengthened with CFRP composites. Fig. 1 shows the cross-sectional details, steel reinforcement layout, and applied loads of the tested beam specimens. Each specimen comprised two equal spans, each of 2850 mm. All beams had a rectangular cross section with a width of 150 mm and a height of 250 mm. The steel reinforcement arrangement was as follows:  $A_{s1} = A_{s2} = 307.9 \text{ mm}^2$ ,  $A_v = 100.5 \text{ mm}^2$ , where  $A_{s1}$  and  $A_{s2}$  are the tensile steel reinforcement amounts in the negative and positive moment regions, respectively, and  $A_v$  is the shear reinforcement of one stirrup. The steel stirrups were spaced at 100 mm center to center. The mechanical properties of the steel used as obtained from three tensile tests on representative specimens, were as follows:  $F_y = 572.6 \text{ MPa}$ ,  $E_s = 192.85 \text{ GPa}$ , and  $\varepsilon_y = 0.3\%$ , where  $F_y$ ,  $E_s$ , and  $\varepsilon_y$  are the average yielding strength, modulus of elasticity, and yielding strain of steel, respectively. The mechanical characteristics of the concrete used for formulating the beams, as obtained from testing eight cylindrical specimens (130 mm  $\times$  260 mm), were as follows:  $f'_c = 39 \text{ MPa}$ ,  $E_c = 29.2 \text{ GPa}$ , and  $f_t = 3 \text{ MPa}$ , where  $f'_c$ ,  $f_t$ , and  $E_c$  are the average compressive strength, tensile strength, and modulus of elasticity of concrete, respectively.

Fig. 2 and Table 1 show the strengthening layout, specimen designations, and details of the control and strengthened beams with EB-CFRP composites. The position of the CFRP reinforcement (either bottom/top or side), the CFRP composite form (either sheet or plate), the CFRP layer number, and the weight of the CFRP sheet were the main variables investigated for this experimental program. Each continuous strengthened beam had the same positive and negative CFRP reinforcement. Each EB beam is identified throughout this paper using a reference code that describes its strengthening scenario. For example, BC1-EB1S means that beam BC1 was strengthened with one externally (E) bonded (B) sheet (S) on the top and bottom surfaces. The number next to the first two letters, BC, indicates the beam number.

In all the tested beams, EB-CFRPs were bonded to the hogging and sagging regions to achieve the highest improvement in the load-carrying capacity. In the hogging region of each specimen, the CFRP reinforcements were placed symmetrically about the central support, whereas, in the sagging regions, the CFRP reinforcements started from the face of the support without any anchorage over the external supports. The strengthening length to the beam length ratio (SL/BL) was considered equal to 0.7 and 0.65 in the hogging and sagging regions, respectively, where SL is the distance between the end of the CFRP and the applied load and BL is the distance between the support and the applied load. To avoid the premature failure of continuous beams with EB-CFRPs, the recommendations outlined in the ACI 440.2R guideline [30] regarding the strengthening length were applied, as shown in Fig. 2b.

Beams BC1-EB1S and BC2-EB1P were tested to study the efficiency of the EB technique through the strengthening material form. Two forms of CFRP were used: sheets (S) and plates (P). Although CFRP sheets and plates have different properties, the axial stiffness ratios of the total reinforcement ( $1 + \frac{E_f \times A_f}{E_s \times A_s}$ ) of BC1-EB1S and BC2-EB1P were designed to be close to each other.

Beam BC3-EB1S-*side* was tested to evaluate the effect of the CFRP sheet's position on the flexural performance of continuous RC beams. The amount of CFRP reinforcement used in this beam was similar to that used in beam BC1-EB1S. However, in the side beam (BC3-EB1S-*side*), the CFRP sheet was cut beforehand in the longitudinal direction of the fibers into two equal halves, and each tension side of the beam was bonded with one half, as shown in Fig. 2.

Beams BC4-EB2S, BC5-EB1S-*weight (700)*, and BC6-EB1S-*weight (1100)* were tested to measure the effect of increasing the EB-CFRP sheet's reinforcement ratio through either the number of layers or the carbon fiber weight on the flexural behavior of the beam. Beam BC4-EB2S was strengthened with two layers of CFRP sheets similar to what has been used in beam BC1-EB1S, whereas, beams BC5-EB1S-*weight(700)* and BC6-EB1S-*weight(1100)* were strengthened with one layer of CFRP sheets weighing 700 g/m<sup>2</sup> and 1100 g/m<sup>2</sup>, respectively. The longitudinal carbon fiber weight of the CFRP sheets applied to beams BC1-EB1S, BC3-EB1S-*side*, and BC4-EB2S was approximately 350 g/m<sup>2</sup>. Fig. 3 shows the three types of CFRP sheets.

Table 2 shows the mechanical properties of the Foreva CFRP sheets and plates used, as provided by the manufacturer. ~~All data were provided by the manufacturer.~~ CFRPs were bonded to the beams using an epoxy-resin adhesive material: Epx TFC (350, 1000) was used for the sheets, whereas Epx SC980 was used for the plates, as shown in Fig. 4. In general, different resin types were used (i) to simulate the real procedure used by construction companies in the field and (ii) to show the workability of Epx TFC resin is higher than that of the Epx SC980 resin, making it more suitable and feasible in case of sheet strengthening. However, Epx TFC 350 is a normal adhesive that usually used for ordinary CFRP sheets (350 g/m<sup>2</sup>), in this study, it was also used for investigating efficiency of the CFRP sheet 750 g/m<sup>2</sup>, whereas Epx TFC 1000 is an epoxy based resin specifically designed to be used with CFRP sheet 1100 g/m<sup>2</sup> structural strengthening systems. Table 3 presents the characteristics of the resin materials.

Table1: Beams details

Beam	Hogging region strengthening			Sagging region strengthening			$A_s$ (mm <sup>2</sup> )	$A_f$ (mm <sup>2</sup> )	$E_f \times A_f$ (kN)	$1 + \frac{E_f \times A_f}{E_s \times A_s}$
	No.	Length	SL/BL	No.	Length	SL/BL				
CB	----	----	----	----	----	----	307.88	----	----	1
BC1-EB1S	1	2.0	0.70	1	2.3	0.65	307.88	72	7560	1.13
BC2-EB1P	1	2.0	0.70	1	2.3	0.65	307.88	56.5	9322.5	1.16
BC3-EB1S- <i>side</i>	1	2.0	0.70	1	2.3	0.65	307.88	72	7560	1.13
BC4-EB2S	2	2.0	0.70	2	2.3	0.65	307.88	144	15120	1.26
BC5-EB1S- <i>weight(700)</i>	1	2.0	0.70	1	2.3	0.65	307.88	99	10395	1.17
BC6-EB1S- <i>weight(1100)</i>	1	2.0	0.70	1	2.3	0.65	307.88	187.5	19635	1.33

Table 2: Characteristics of the CFRP composites

Material	Width ×Depth (mm×mm)	Ultimate strength (MPa)	Modulus of elasticity (GPa)	Strain at failure (%)
CFRP-Sheet-350 g/m <sup>2</sup>	150×0.48	1700	105	1.7
CFRP-Sheet-700 g/m <sup>2</sup>	150×0.66	1700	105	1.7
CFRP-Sheet-1100 g/m <sup>2</sup>	150×1.25	1700	105	1.7
CFRP-Plate	50×1.2	2800	165	1.7

Table 3: Characteristics of the epoxy-resin

Material	Compressive strength (MPa)	Tensile strength (MPa)	Elastic modulus (GPa)
Epoxy resin- SC980 [22]	83	29.5	4.94
Epoxy resin-TFC (350)	89	27	2.3
Epoxy resin-TFC (1000)	68	48	1.7

### 2.1.2 Beams strengthened with NSM CFRP reinforcements

For the **purpose** sake of comparison, two additional beams, namely BC1-NSM and BC2-SNSM, were strengthened using the NSM technique and statically tested. ~~The procedure followed in the NSM technique is described elsewhere [9]. The experimental results of the two beams mentioned above were compared with the experimental results of beams BC1-EB1S and BC3-EB1S side from Section 2.1.1.~~ Beams BC1-NSM and BC2-SNSM were strengthened with 2Ø6 CFRP rods in both the hogging and sagging regions. The only difference between them was the location of the CFRP bars. In beam BC2-SNSM, the CFRP bars were inserted in the vertical sides adjacent to the tension steel rebars instead of the bottom/top sides, as shown in Fig. 5. The dimensions, steel reinforcement ratio, and test setup, including the load and support conditions of the NSM beams, were all comparable **similar** to those employed in the experimental investigation of the EB beams, as shown in Fig. 1. In addition, the mechanical properties of the adhesive epoxy-resin (Epx SC980) used to bond the CFRP bars with concrete were similar to those reported in Table 3. The ultimate strength and elastic modulus of the CFRP bars used were equal to 2800 MPa and 165 GPa, respectively.

Table 4 presents the strengthening details of the NSM beams. Their axial stiffness ratio was found to be approximately 1.16, which is slightly larger than that recorded for EB beams (i.e. 1.13; see Table 1), although the area of the CFRP bars used in BC1-NSM and BC2-SNSM (2Ø6 = 56.5 mm<sup>2</sup>) was smaller than that of the sheet used in BC1-EB1S and BC3-EB1S-side (one sheet = 72 mm<sup>2</sup>).

Table 4: Details of the NSM-CFRP bar beams

Beam	Hogging region strengthening			Sagging region strengthening			$A_s$ (mm <sup>2</sup> )	$A_f$ (mm <sup>2</sup> )	$E_f * A_f$ (kN)	$1 + \frac{E_f * A_f}{E_s * A_s}$
	No.	Length	SL/BL	No.	Length	SL/BL				
BC1-NSM	2Ø6	2.0	0.70	2Ø6	2.3	0.65	307.88	56.5	9322.5	1.16

BC2-SNSM	2∅6	2.0	0.70	2∅6	2.3	0.65	307.88	56.5	9322.5	1.16
----------	-----	-----	------	-----	-----	------	--------	------	--------	------

## 2.2. Surface preparation and strengthening technique

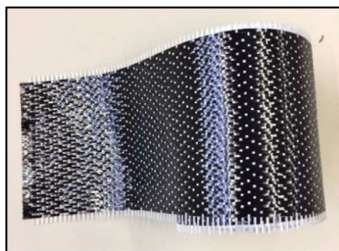
Regarding the beam specimens strengthened with EB CFRP sheets, a concrete surface was prepared first using a mechanical grinder, as shown in Fig. 6a. Then the surface was cleaned with compressed air to remove debris and fine particles (Fig. 6b). Next, an initial layer of Epx TFC epoxy was added and distributed over the prepared concrete surface using a paint roller (Fig. 6c). The CFRP sheets were saturated with an epoxy resin while being installed, and the paint roller was applied with a considerable amount of pressure to roll the CFRP sheets in the longitudinal direction of the fibers, as illustrated in Fig. 6d. This was done to ensure proper bonding between the CFRP sheets and the concrete substrate.

Regarding the beam specimen strengthened with CFRP plates, the same procedure described above was applied. The only difference was the type of epoxy resin used; that is Epx SC980 was used for the plated beams instead of Epx TFC. The final shape of the CFRP plated beam is shown in Fig. 6e.

Regarding the beam specimens strengthened with NSM CFRP bars, the procedure followed in the NSM technique has already been described in Ref. [9]. For all the strengthened specimens, the CFRP composites were allowed to cure for seven days before testing.

## 2.3. Instrumentation and test setup

One control beam, four beams strengthened with one EB sheet, one beam strengthened with two-layer sheets, and one beam strengthened with one EB plate, and two beams were strengthened with NSM CFRP bars were loaded until destruction with two concentrated loads separated by a distance of 2850 mm. For the loading process, two hydraulic actuators with a capacity of 400 kN and an average loading speed of 0.3 kN/s were used. The total applied load, central support reaction, midspan deflection, and strain of the steel and CFRP were measured during the tests. The reaction at the interior support was measured using a load cell with a capacity of 200 kN, while two vertical linear variable differential transducers (LVDTs) were used for each beam to monitor the vertical midspan deflection (one LVDT at each midspan). The tested beam specimens were instrumented with electrical strain gauges attached to the tension steel and CFRP at the central support and midspan sections to measure their tensile stresses. Fig. 7 illustrates the instrumentations used and the bending test setup.



a) CFRP sheet (350g/m<sup>2</sup>)

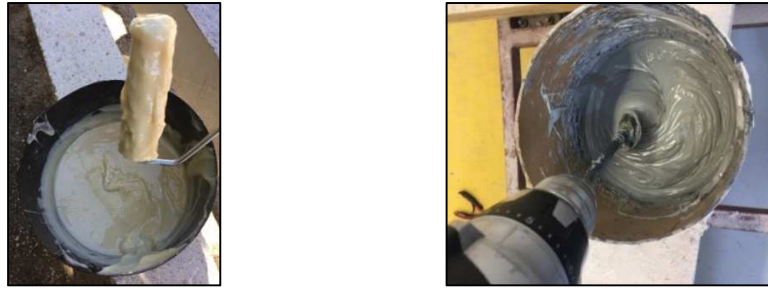


b) CFRP sheet (700g/m<sup>2</sup>)



c) CFRP sheet (1100g/m<sup>2</sup>)

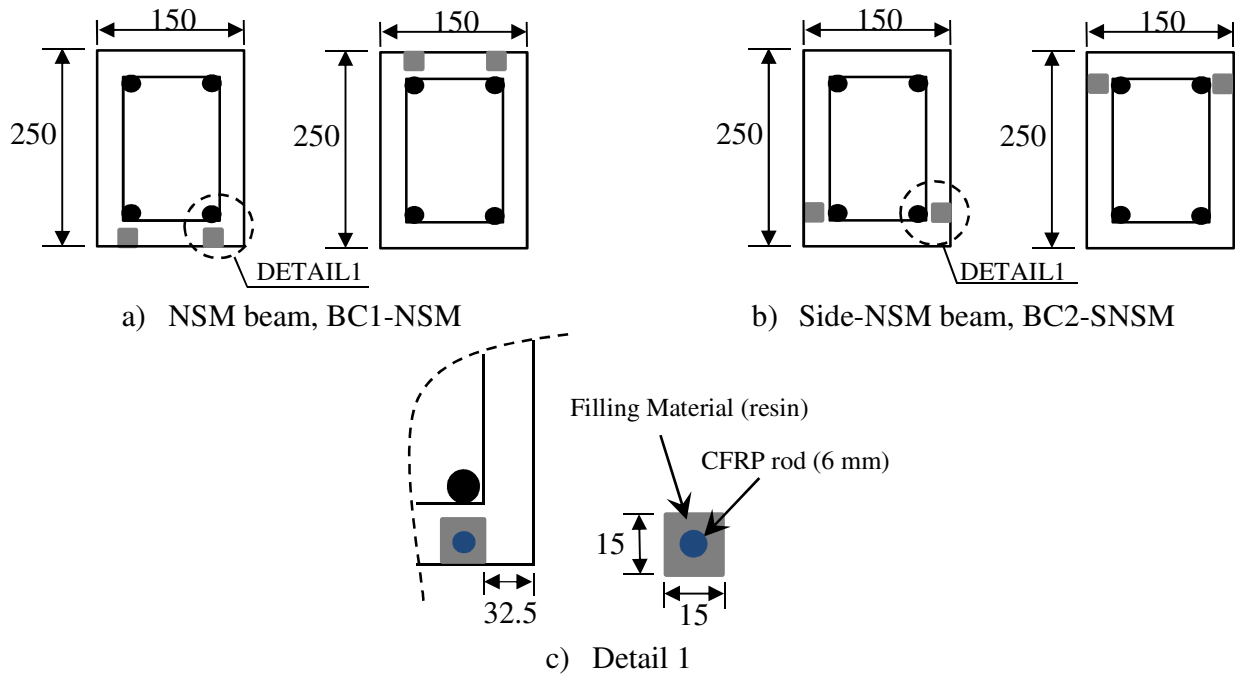
Fig. 3: CFRP sheets used for strengthening beams



(a)

(b)

Fig. 4: Epoxy resin material for bonding the CFRP (a) sheets and (b) plates



a) NSM beam, BC1-NSM

b) Side-NSM beam, BC2-SNSM

c) Detail 1

Fig. 5: Cross-section and groove dimensions details of NSM beams (all dimensions are in mm)



(a)

(b)

(c)

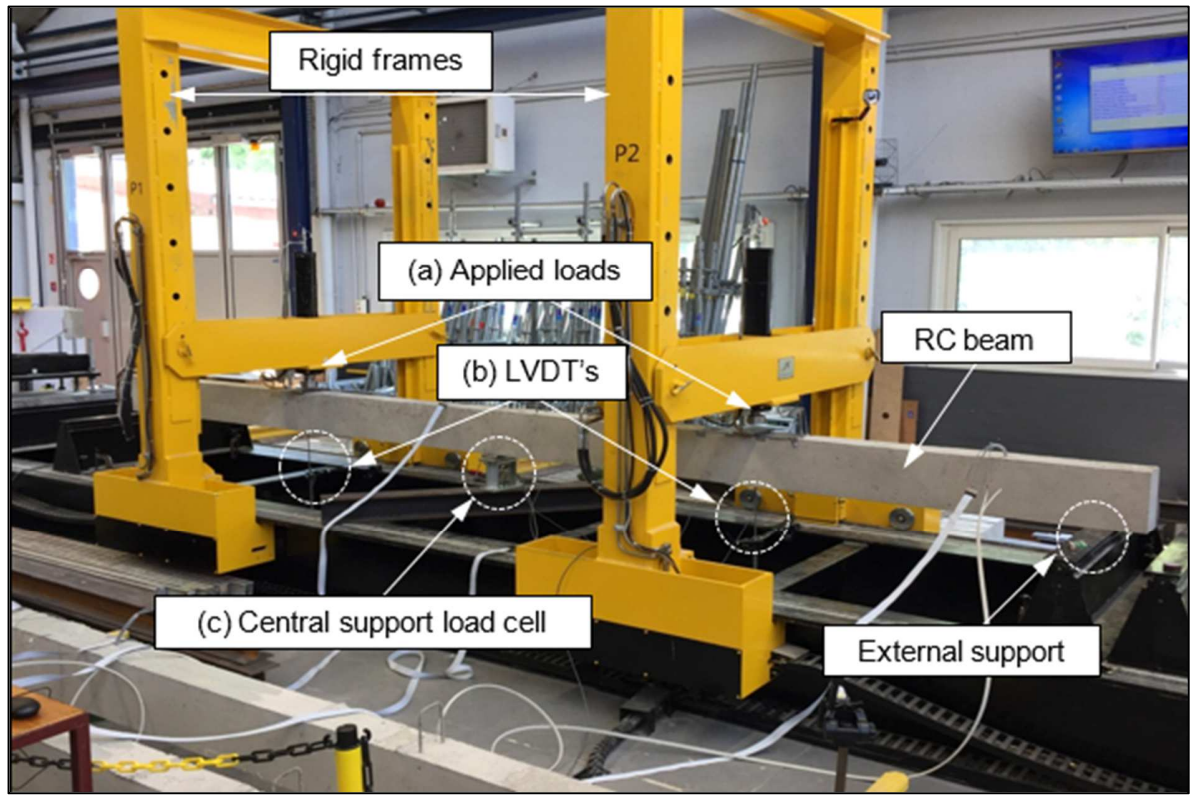
(d)

(e)

(a) Preparing the concrete surface, (b) Cleaning the concrete surface, (c) Adding initial layer of epoxy, (d)

Installing the CFRP sheet, and (e) Final shape of beam strengthened with CFRP plates.

**Fig. 6: Strengthening procedure of EB-CFRP beam specimens**



(a) Applied load



(b) LVDT



(c) Central support

Fig. 7: Instrumentation and test setup



### 3. Results and Discussion

#### 3.1 Beams strengthened with EB CFRP reinforcements

##### 3.1.1 Load-deflection response

Fig. 8 presents the applied load versus the midspan deflection of the control and strengthened beams. The load-deflections curves of the tested beams typically consist of three stages: the precracking of concrete, postcracking of concrete, and postyielding of steel. No noticeable remarkable variation was found between the beams at the first stage. By In contrast, the comparisons provided in Fig. 8 show increases in the postcracking stiffness, load at yielding, and load at failure in the EB-CFRP beams in comparison to the control beam. Such increases were principally controlled by the number of layers, by the form and weight of the carbon fibers, and marginally by the position of the CFRP reinforcement. Indeed, among all the tested strengthened specimens, the highest improvement in the load-deflection response was achieved in the beam employing one layer of 1100 g/m<sup>2</sup> CFRP sheet (BC6-EB1S-weight (1100)), whereas the lowest improvement was reported in the beam strengthened with CFRP plates (BC2-EB1P). Overall, in all the tested beams, the increasing percentages of the yield and ultimate load due to the EB-CFRP composites were found to range from 25.5% to 59.1% and from 7.6% to 49.8%, respectively.

The ultimate load of beams BC1-EB1S (219.4 kN) and BC4-EB2S (242.4 kN) was found to be about 29.3% and 42.8 higher than that of the control beam (169.7 kN), respectively. This result confirms that increasing the amount of CFRP reinforcement using multisheet layers contributes is considerably responsible for to the enhancing of the load-carrying capacity of continuous beams, as one can also notice in Ref. was also evidenced in [8].

It has also been observed that the efficiency of the EB-CFRP plate in improving the flexural strength of continuous beams in terms of the ultimate load capacity was lower than that observed for the EB-CFRP sheets. Although the axial stiffness ratio of beam BC2-EB1P (1.16) was slightly greater than that of beam BC1-EB1S (1.13), the ultimate load capacity of BC2-EB1P (182.52 kN) was only 83% that of BC1-EB1S. This lower efficiency of the EB-CFRP plates may attributed to the bonding surface between the CFRP and the concrete substrate. The bonding surface between the CFRP sheet and the concrete surface in beam BC1-EB1S (width of sheet: 150 mm) was about three times that between the CFRP plate and the concrete in beam BC2-EB1P (width of plate: 50 mm). Therefore, it may conclude that the bonding area is more influent than the axial stiffness ratio when the comparison on the basis of the EB-CFRP form.

The load-deflection graphs (Fig. 8) also show that the side-bonded CFRP sheet was slightly less efficient than the conventional top/bottom-bonded CFRP sheets in terms of enhancing the flexural behavior of continuous RC beams, making it a feasible alternative. Compared to beam BC1-EB1S, the decrease in the ultimate load (205.43 kN) of beam BC3-EB1S-side was only 6.4%. This difference in the load-carrying capacity is most likely due to the decrease in the effective moment arm depth of the tension reinforcements in beam BC3-EB1S-side due to the changing position of the CFRP sheet.

Because the CFRP reinforcement area was higher, it was expected that the load-carrying capacity of beam BC5-EB1S-weight(700) would be relatively higher than that of beam BC1-

EB1S. However, this hypothesis **expectation** was not confirmed by beam BC5-EB1S-*weight(700)*, as can be discerned from Fig. 8d. Although the postyielding stiffness **was** improved, increasing the carbon-fiber weight from 350 g/m<sup>2</sup> to 700 g/m<sup>2</sup> **was** found **to** not to allow an additional improvement in the ultimate load capacity of the beam. The failure load of beam BC5-EB1S-*weight(700)* (217.6 kN) was about 99.2% of the failure load of beam BC1-EB1S. This can be attributed to (i) increasing the CFRP reinforcement from 72 mm<sup>2</sup> in BC1-EB1S to 99 mm<sup>2</sup> in BC5-EB1S-*weight(700)* **was** not being sufficient to significantly increase the axial stiffness ratio, which remains very close in the two beams (1.13 in BC1-EB1S and 1.17 in BC5-EB1S-*weight(700)*); and (ii) the adhesive epoxy-resin used, Epx TFC 350, **was** not being suitable to saturate heavy and dense carbon fiber fabrics such that used in BC5-EB1S-*weight(700)*.

The impact of increasing the carbon-fiber weight can be clearly seen in beam BC6-EB1S-*weight(1100)*, where the failure load (254.26 kN) increased by 49.8% over that of the control beam and even by 4.9% over that of the beam strengthened with two sheet layers (i.e. BC4-EB2S, 350 g/m<sup>2</sup>), (Figs. 8c and 8d). The CFRP reinforcement amount and the axial stiffness ratio of BC6-EB1S-*weight(1100)* were 1.3 and 1.06 times those in BC4-EB2S. It should be noted that a special soft adhesive (Epx TFC 1000) was used in BC6-EB1S-*weight(1100)* to ensure saturation such a heavy carbon sheet.

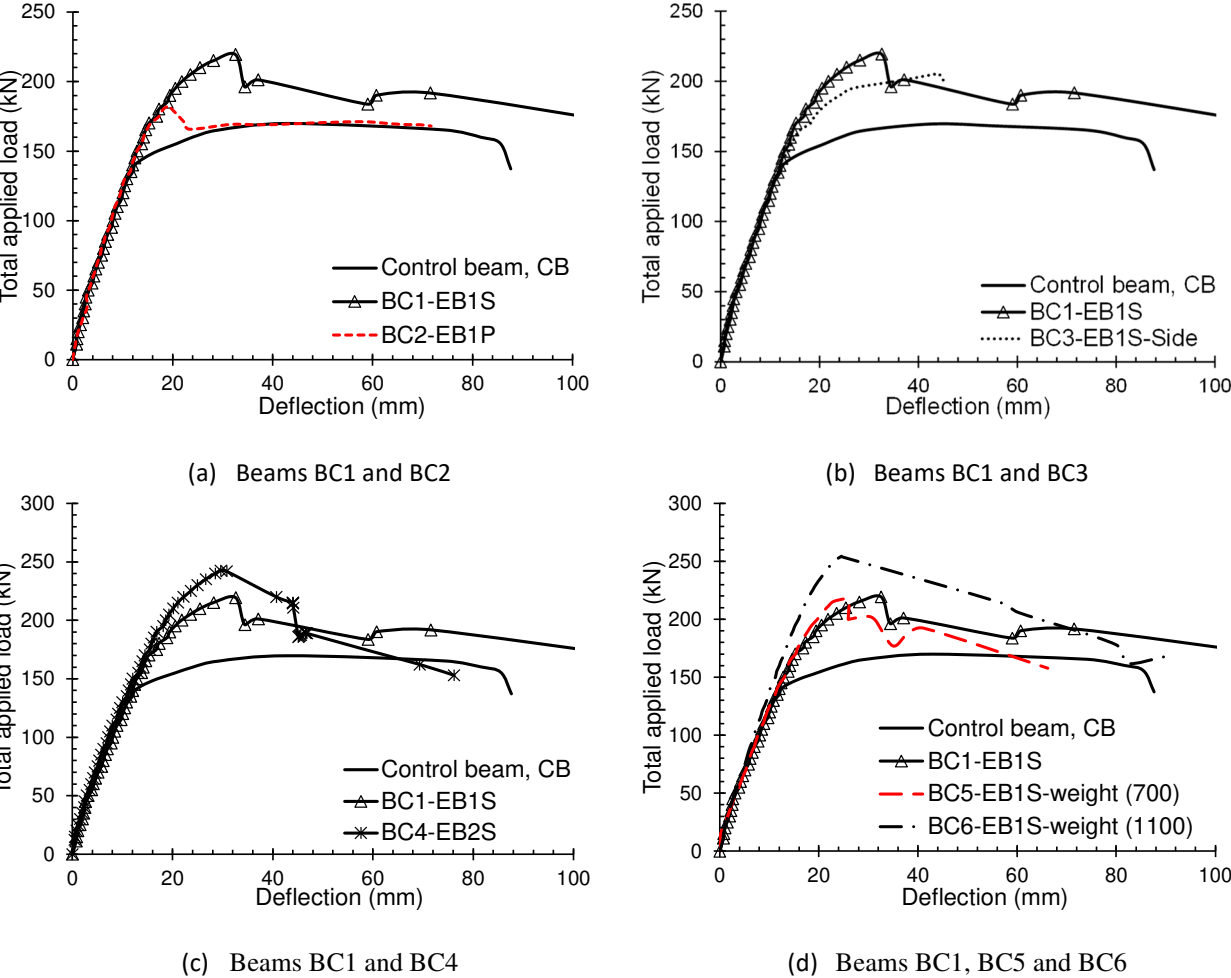


Fig. 8: Load deflection curves of tested beams

3.1.2. Failure modes

Four failure modes were observed in the tests (i) conventional flexural failure, (ii) IC debonding of CFRP plates/sheets, (iii) IC debonding of CFRP sheets in one region followed by concrete cover delamination (CCD) in the other region, and (iv) IC debonding of CFRP sheets followed by tensile rupture of the CFRP sheets. ~~These failure modes are described in detail in the following sections.~~

Debonding of CFRP sheets and plates as a result of ICs at critical sections (midspan and over the central support) was the dominant failure mode observed in the strengthened beams. IC debonding appeared to be the only failure mode in beams BC2-EB1P and BC6-EB1S-*weight(1100)*, whereas it was followed by other types of failure, such as CCD, in beams BC1-EB1S, BC4-EB2S, and BC5-EB1S-*weight(700)*, as well as tensile rupture of CFRP sheets in beam BC3-SEB1S-*side*. Such debonding of the CFRP composites as a results of ICs started first either at the midspan or over the central support and then developed toward the ends of the CFRP composites with the increase of the external applied load. By contrast, in the regions that failed as a result of CCD, separation of the concrete cover started at the ends of the CFRP composites due to the formation of diagonal flexural shear cracks and then propagated toward the interior critical section.

It worth noting ~~should be noted~~ that the separation of the EB-CFRP sheets/plates observed in the tested beams, resulting from either IC or CCD failures, occurred with concrete attached, meaning that it was accompanied by a loud noise and dust. In all the tested CFRP beams, ripping and limited crushing of the compressed concrete at the external load application sections and central support occurred before the EB-CFRP failure.

3.1.2.1 Failure mode 1: Conventional ductile flexural failure

This failure mode was illustrated by the control beam specimen (CB), as shown in Fig. 9. This failure started by the yielding of the tension steel reinforcement followed by concrete crushing in the compression surfaces at the central support and points of the applied loads.

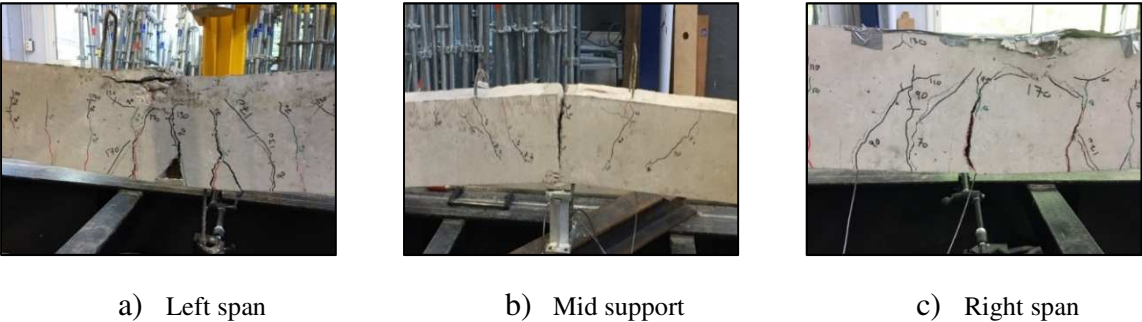


Fig. 9: Failure mode of control beam, CB.

3.1.2.2 Failure mode 2: IC debonding

Debonding failure of EB-CFRP resulting from an IC was demonstrated by beams BC2-EB1P and BC6-EB1S-*weight(1100)*, as shown in Figs. 10 and 11, respectively.

The IC debonding in beam BC6-EB1S-weight (1100) **was** first occurred in the left sagging region, followed by failure of the hogging and right sagging regions. In beam BC2-EB1P, the IC debonding occurred simultaneously at the hogging and left sagging regions. This IC debonding was explosive and was followed immediately by beam failure.

Interestingly, such debonding failure was not observed in the right span of beam BC2-EB1P. This was most likely associated with the IC width, which was considerably greater in the left span and over the central support than in the right span. However, the CFRP plates were rapidly affected by the development of ICs at the critical sections because of the small contact area between the EB-CFRP plate and the concrete. This led to the acceleration of the debonding phenomena, thus explaining the lower ultimate capacity of this beam in comparison to that of beam BC1-EB1S (Section 3.1.1).

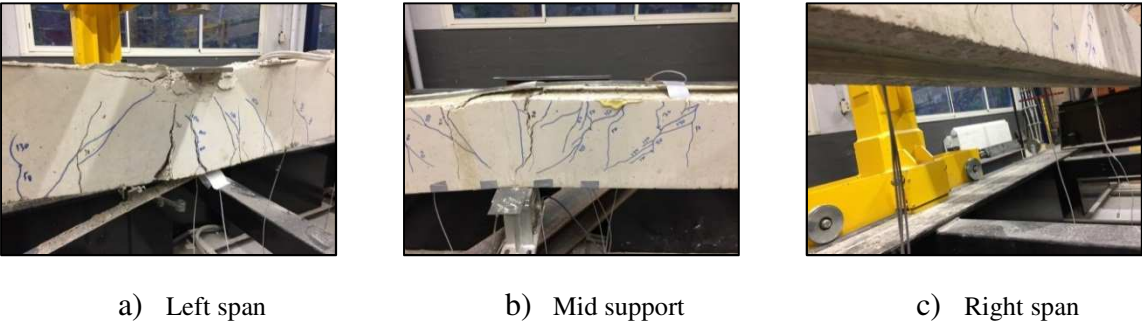


Fig. 10: Failure mode of beam BC2-EB1P.

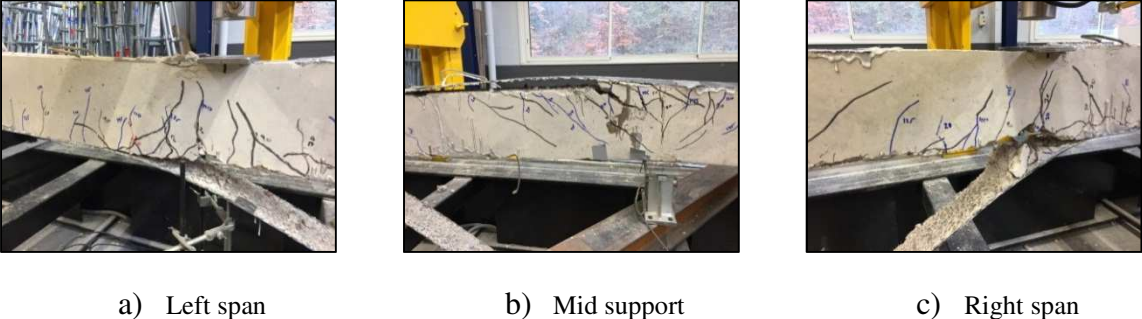


Fig. 11: Failure mode of beam BC6-EB1S-weight(1100).

3.1.2.3 Failure mode 3: IC debonding and CCD

Beam BC1-EB1S failed in two areas as a result of IC debonding of the EB-CFRP sheets: firstly at the negative moment zone (hogging region) close to the central support and then again in the left positive moment zone (sagging region). During later stages, the beam failed **followed** by CCD at the right positive moment zone. The failure that occurred at the hogging region was sudden and was accompanied by a loud noise, indicating rapid release of energy and significant loss in the load capacity (see Fig. 8). In the right sagging region, however, delamination of the concrete cover started at the extremities of the CFRP sheets close to the external supports and developed toward the applied load points with the load increasing. This

was accompanied by a loud cracking noise, which continued until the end of the test. Fig. 12 shows the failure mode of beam BC1-EBS.

In beams BC4-EB2S and BC5-EB1S-weight (700), IC debonding occurred in the left sagging region and then in the hogging region, followed by CCD in the right sagging region, as shown in Figs. 13 and 14. This failure mode—may indicates that increasing the reinforcement ratio of the EB-CFRP sheets through the number of layers and carbon-fiber weight (see also Section 3.1.2.2) is not effective in terms of preventing the IC debonding.

3.1.2.4 Failure mode 4: IC debonding and rupture of the CFRP sheet

Beam BC3-SEB1S-side principally failed as a result of IC debonding of the EB-CFRP sheets at both the hogging and sagging regions. Debonding failure was first observed in the left sagging region, followed by failure of the hogging and right sagging regions. This IC debonding failure resulted in a tensile rupture of the CFRP sheets at the critical sections, as shown in Fig. 15. Such an abrupt rupture of the CFRP sheets occurred because once the CFRP sheets were debonded from one side of the beam, the load suddenly transferred to the other side.

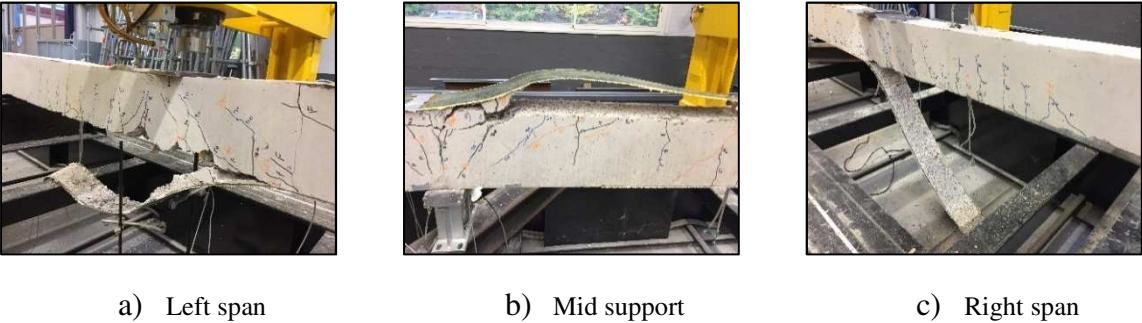


Fig. 12: Failure mode of beam BC1-EB1S

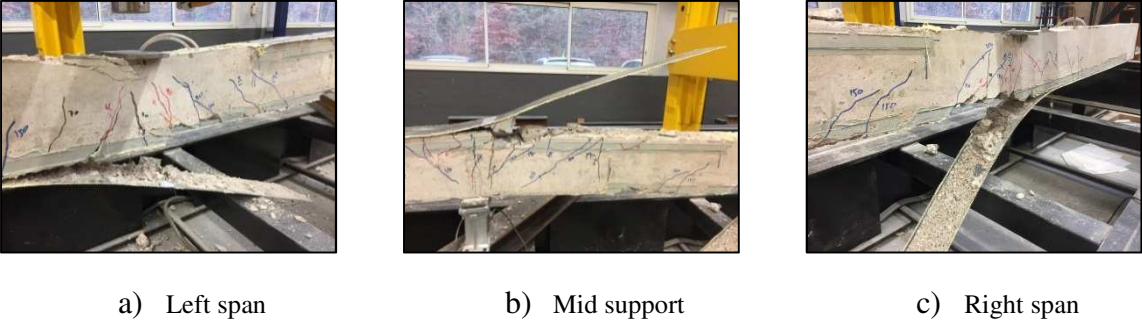


Fig. 13: Failure mode of beam BC4-EB2S

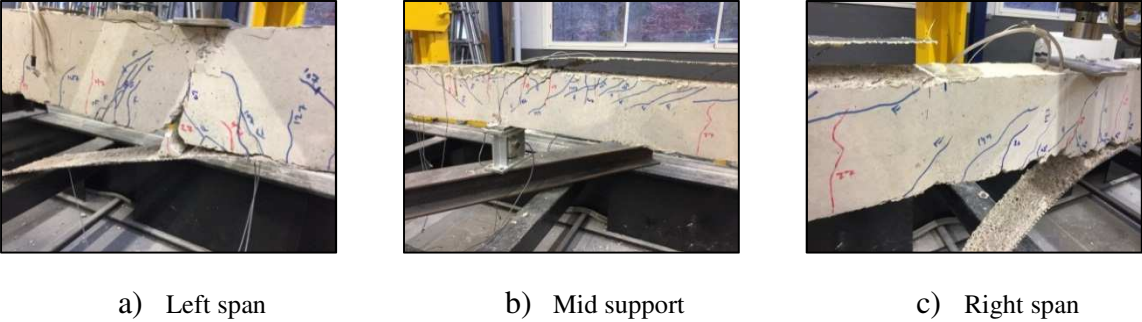


Fig. 14: Failure mode of beam BC5-EB1S-weight(700)



Fig. 15: Failure mode of beam BC3-SEB1S-side

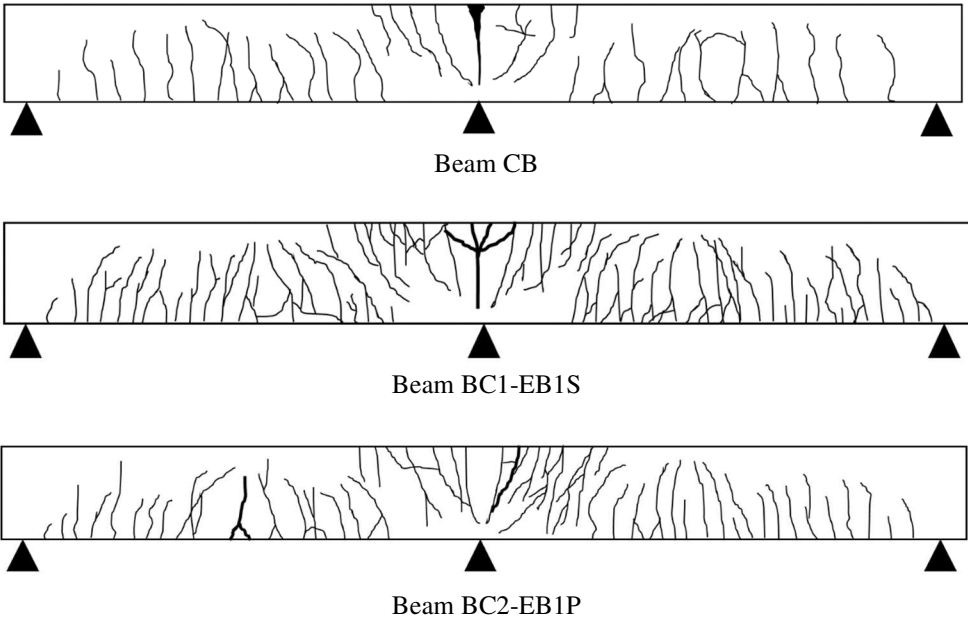
### 3.1.3 Crack maps and crack width

Fig. 16 shows the cracks maps of strengthened and unstrengthened beams at the failure stage. ~~Crack propagation was monitored and manually marked throughout the tests.~~ The ICs ~~at the critical sections (maximum moment regions)~~ are depicted by bold lines to reflect their larger width compared to other cracks. The ICs started nearly simultaneously in both the hogging and sagging regions in all the tested beams. However, as can be seen in Fig. 16, strengthening a continuous RC beam with EB-CFRP significantly increased the number of cracks, regardless of the strengthening state. Compared to the control beam, the number of cracks increased by 189%, 200%, 63%, 125%, 213%, and 238% in the hogging region and by 125%, 44%, 19%, 19%, 44%, and 63% in the sagging region for beams BC1-EB1S, BC2-EB1P, BC3-EB1S-side, BC4-EB2S, BC5-EB1S-weight (700), and BC6-EB1S-weight (1100), respectively. In addition, the average crack spacing of the EB beams was found to be smaller than ~~that~~ in the control beam. In general, the average crack spacing is calculated by summing the crack spaces divided by the number of spaces in each region, and it was found to be equal to 163, 80.2, 88.5, 88.3, 82.5, 86.6, and 86.6 mm in the hogging region and 136, 85.2, 94.3, 107.9, 115, 103.9, and 102.1 mm in the sagging region for beams CB, BC1-EB1S, BC2-EB1P, BC3-EB1S-side, BC4-EB2S, BC5-EB1S-weight (700), and BC6-EB1S-weight(1100), respectively.

Beams BC4-EB2S and BC6-EB1S-weight(1100) exhibited a higher first cracking load than that experienced by other beams due to their high axial stiffness ratio. The first cracking loads of beams CB, BC1-EB1S, BC2-EB1P, BC3-EB1S-side, BC4-EB2S, BC5-EB1S-weight (700), and BC6-EB1S-weight (1100) were found to be approximately 26, 30, 29, 32, 46, 30, and 52 kN respectively. Therefore, it can be concluded that the axial stiffness ratio of the EB-CFRP specimen is the key factor affecting the first crack load.

At later stages of loading, the influence of the strengthening scenarios applied could be noticed through the crack width of the specimens. Fig. 17 shows the relationship between the total applied load and the flexural crack width in the hogging region. The crack width was measured using a special microscope with an accuracy of 0.05 mm. Generally, EB-CFRP sheets/plates have a considerable effect on reducing the width of flexural cracks. Nevertheless, the crack width of the CFRP sheet beams (i.e. BC1-EB1S, BC3-EB1S-side, BC4-EB2S, BC5-EB1S-weight (700), and BC6-EB1S-weight (1100)) was ~~found to be~~ significantly smaller than that of the CFRP plate beam (i.e. BC2-EB1P) under the same applied load. This finding indicates that not only the axial stiffness ratio of the EB-CFRP specimen, but also the form and position of the CFRP may affect the crack development. Indeed, bonding the CFRP sheets on the side surfaces of the beam (BC3-EB1S-side) was found to be more efficient in decreasing the beam’s crack width than the conventional top/bottom bonding technique (BC1-EB1S). This can be explained as the side-bonded sheets confine the concrete in the tension sides along the depth of the beam’s cross section, which allows enhancing the tension carrying capacity of concrete between cracks.

The red points shown in Fig. 17 represent the maximum crack width in each strengthened beam corresponding to the service load (67% ultimate load). According to ACI-319-14 [35], the allowable crack width of ordinary steel RC beams ranges between approximately 0.46 and 0.56 mm at the service load. It can be seen from Fig. 17 that none of the CFRP sheet beams exceeded the maximum limit (0.56 mm). Moreover, beams BC3-EB1S-side, BC4-EB2S, BC5-EB1S-weigh (700), and BC6-EB1S-weigh (1100) did not even exceed the lower crack width limit (0.46 mm). These results highlight the great benefits of using EB-CFRP sheets and their strengthening configurations adopted in this study to meet the serviceability requirements of continuous RC beams in comparison to the control and EB-CFRP plate beam.



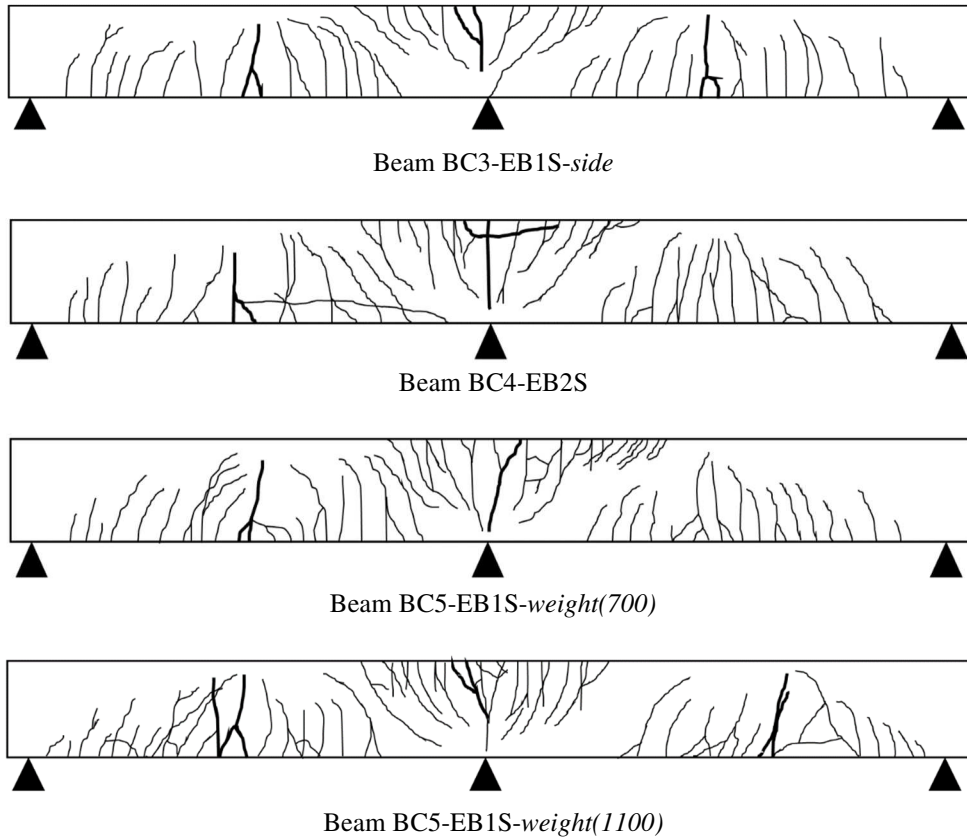


Fig. 16: Crack maps of tested beams

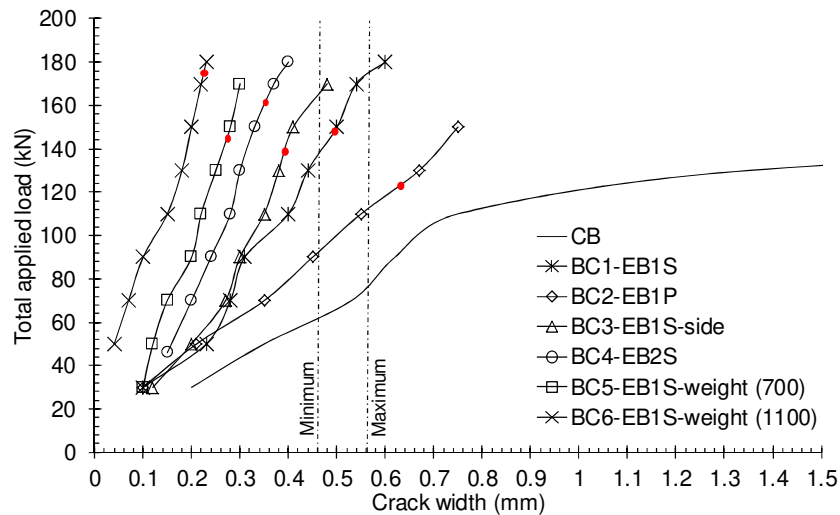


Fig. 17: Total applied load vs. the cracks width of control and strengthened beams

### 3.1.4 Strain of steel and CFRP reinforcement

Fig. 18 shows the total applied load versus the tensile strain of the bottom steel bars at the midspan (sagging region) and the top steel bars at the intermediate support (hogging region). Besides acting as tensile reinforcements, EB-CFRP composites have also been demonstrated to be useful in reducing the tensile strain of tension steel bars. Under the same level of applied load, and compared to the control beam, the steel strain decreased in both the hogging and



sagging regions of the EB beams. The intensity degree of this decrease varies depending on the form, position, and number of CFRP sheets used, as well as the weight of the carbon fibers.

In general, the strain response of tension steel bars is affected by two characteristic points: the concrete cracking load point, which has been discussed in the previous section, and the steel yielding load point. It can be seen in Fig. 18 that the EB-CFRP composite material delayed the yield of the steel bars. Thus, both the yield and the ultimate load of the strengthened beam increased in comparison to those of the control beam. It was also observed that steel yielding ( $\epsilon_s > 0.003$ ) occurred in all the strengthened beams prior to the debonding failure of the CFRP. Although such yielding was comparable in both the hogging and sagging regions because the amount of reinforcement used was the same, most of the tested beams exhibited their first yielding in the hogging region. Thus, the comparisons provided below are based on the yielding load of tension steel in the hogging region.

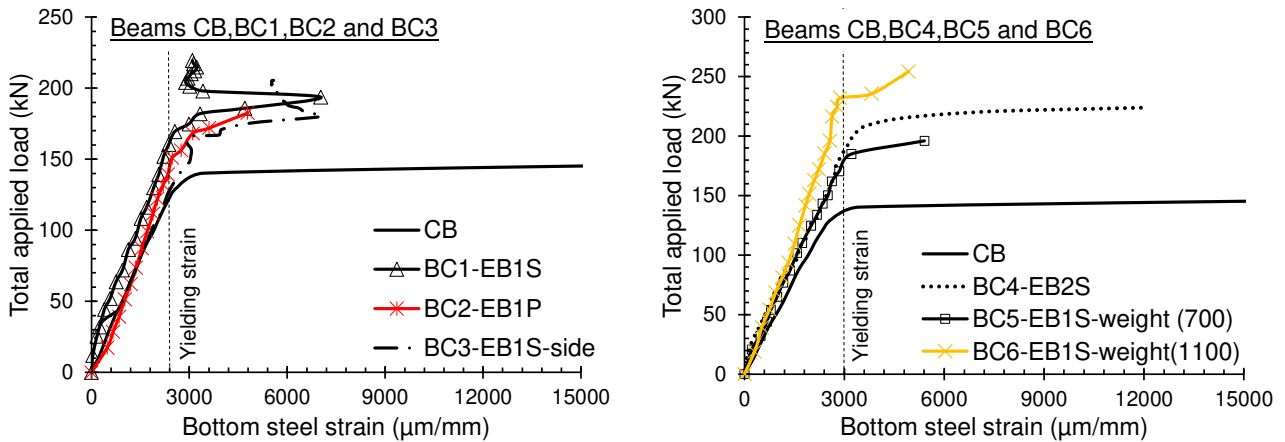
- *Influence of the axial stiffness ratio:* The load-strain diagrams show that both forms of CFRP (sheets and plates) allow an increase in the yielding load. This increase was found to be approximately 29.6% and 29.2% for beams BC1-EB1S (171.4 kN) and BC2-EB1P (170.9 kN), respectively. Such similarity in the yielding load values of the aforementioned beams, despite the different forms of CFRP used, is most probably due to the affinity of the axial stiffness ratio, which is nearly 1.13 in BC1-EB1S and 1.16 in BC2-EB1P. Similarly, the yielding loads of beams BC4-EB2S (190 kN), BC5-EB1S-weight (700) (172.2 kN), and BC6-EB1S-weight(1100) (210.5 kN) increased by 43.6%, 30.2%, and 59.1% respectively, over the control beam. The axial stiffness ratio of beams BC4-EB2S, BC5-EB1S-weight (700), and BC6-EB1S-weight (1100) was about 1.26, 1.17, and 1.33, respectively. It was also found that positioning the CFRP sheets on the side instead of the bottom/top surfaces has a negligible effect. Although the position of the CFRP has changed, the yielding load of BC3-EB1S-side (166.1 kN) was about 97% that of BC1-EB1S. The axial stiffness ratio of beam BC3-EB1S-side was similar to that of beam BC1-EB1S. Fig.19 shows the relationship between **increasing** the axial stiffness ratio and the yielding load of EB-CFRP beams.

Fig. 20 shows a plot of the total applied load versus tensile strain in the CFRP composites at the midspan and over the intermediate support of the tested beams. The maximum recorded tensile strain values in the CFRP materials obtained from the experimental investigations of beams BC1-EB1S, BC2-EB1P, BC3-EB1S-side, BC4-EB2S, BC5-EB1S-weight (700), and BC-EB1S-weight (1100) were found to be, respectively, 0.0113 (66%), 0.005 (29.4%), 0.0114 (67%), 0.0068 (40.1%), 0.0082 (48%), and 0.0069 (40.4%) at the midspan and 0.0082 (48%), 0.0061 (35.9%), 0.0106 (62%), 0.0075 (44.2%), 0.0085 (49.8%), and 0.0051 (30.2%) at the intermediate support. The values in parentheses represent the percentages of the maximum recorded strain ( $\epsilon_{FRP}^{max}$ ) to the ultimate strain ( $\epsilon_{FRP}^{ult}$ ) of the CFRP. On the basis of the above results, the following points can be made:

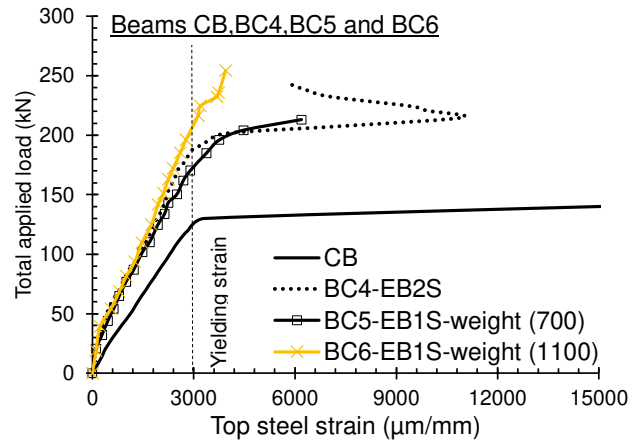
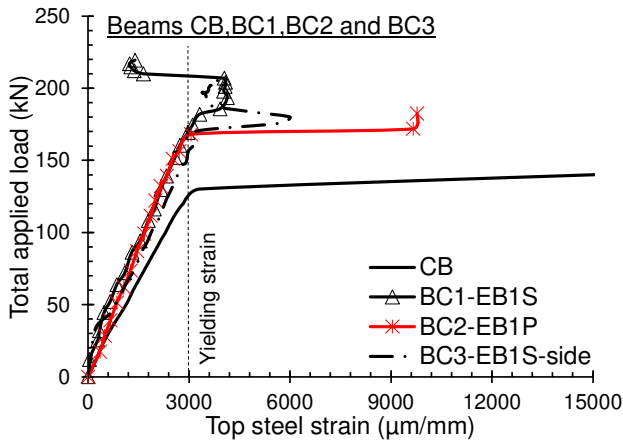
- *Influence of the CFRP form:* Using EB-CFRP plates instead of EB-CFRP sheets significantly decreases the maximum tensile strain of CFRP and, hence, decreases the probability that its capacity could be further exploited. Such decrease is due to the

early IC debonding failure that was observed in the plated beam in comparison to the sheeted beam, as discussed in Section 3.1.2.2.

- *Influence of the CFRP sheet position:* Among all the tested beams, the largest maximum strain was achieved by bonding CFRP sheets to the side surfaces of beam BC3-EB1S-side. It should be noted that, in the side-bonded beam, the tensile stress distribution of CFRP varies along the width of the sheets. This variation allows the extreme top carbon fibers in the hogging region and the extreme lower carbon fibers in the sagging region to elongate rapidly before the global debonding failure occurs, as presented in Figs.20c and 20d. ~~This variation between the strains of the top and bottom carbon fibers in beam BC3-EB1S-side is also presented in Figs.20e and 20d.~~
- *Influence of the CFRP sheet area:* Increasing the CFRP reinforcement area through the number of CFRP sheet layers (BC4-EB2S) and the weight of the carbon fibers (BC5-EB1S-weight(700) and BC6-EB1S-weight(1100)) was found to have a similar impact on the maximum strain of EB-CFRP sheets ( $\epsilon_{FRP}^{max}$ ). Both process significantly decreased the value of  $\epsilon_{FRP}^{max}$  in the hogging and sagging regions. For example the debonding strain of CFRP sheet in the hogging region decreased from 0.0113 in beam BC1-EB1S to 0.0068, 0.008, and 0.0069 in beams BC4-EB2S, BC5-EB1S-weight (700), and BC5-EB1S-weight (1100), respectively. The relationship between increasing the CFRP reinforcement area and debonding strain is presented in Fig. 21. This relationship was found to be nonlinear for both hogging and sagging regions.



(a) Bottom steel



(b) Top steel

Fig. 18: Total applied load versus tensile strain of the steel bars

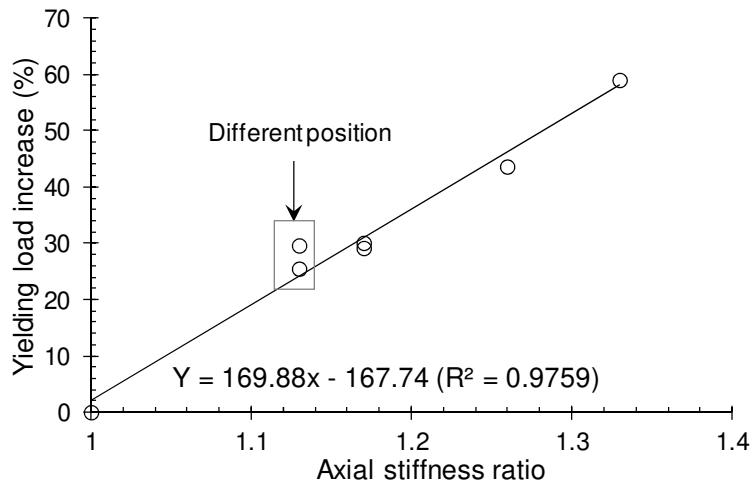
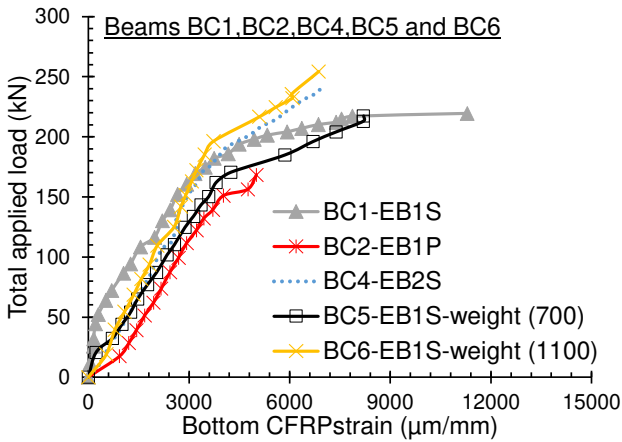
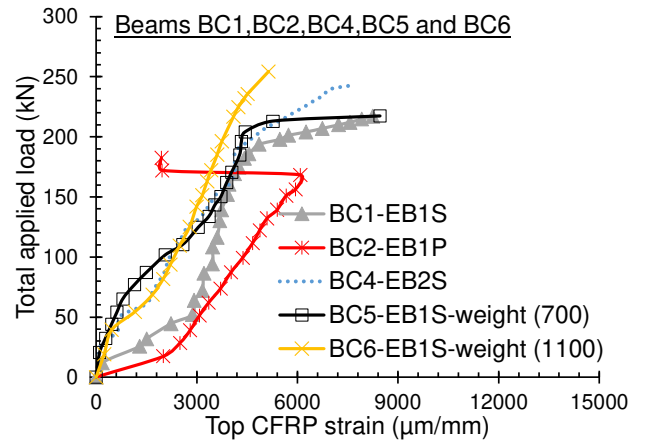


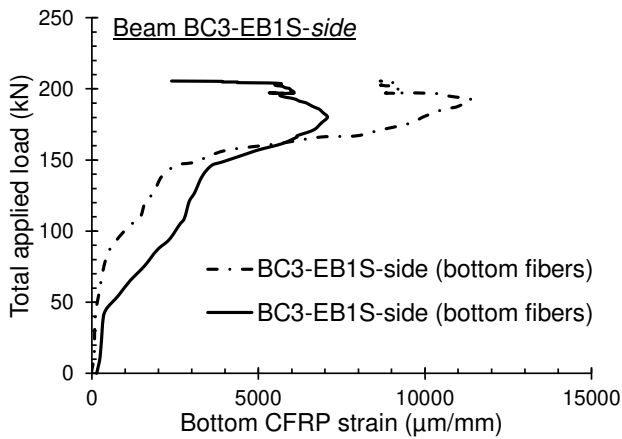
Fig. 19: Axial stiffness ratio vs. increasing the yielding load



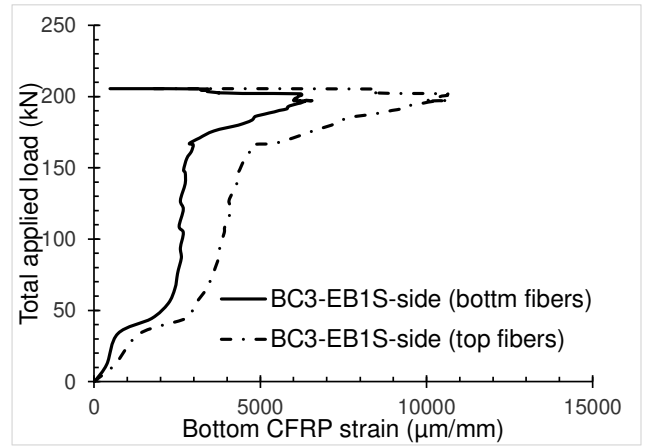
(a) Bottom CFRP, beams BC1, BC2, BC4 and BC5



(b) Top CFRP, beams BC1, BC2, BC4 and BC5



(c) Bottom CFRP, beam BC3



(d) Top CFRP, beam BC3

Fig. 20: Total applied load versus tensile strain of CFRP reinforcement

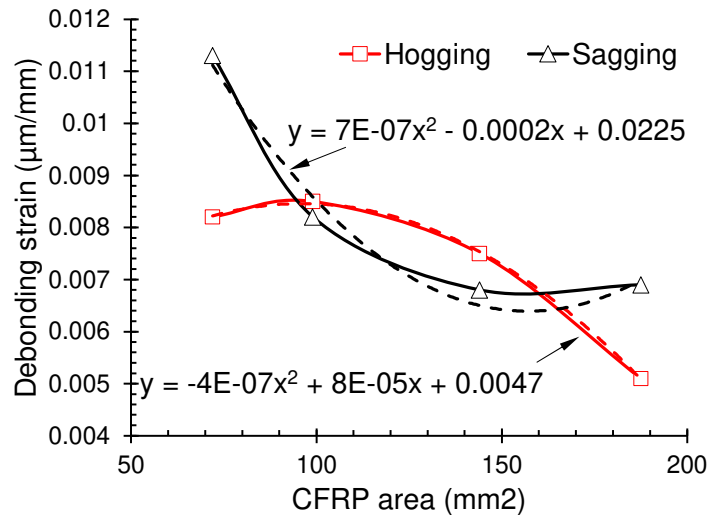


Fig. 21: CFRP sheet area vs. debonding strain

### 3.1.5 Moment redistribution

Although a considerable number of studies have addressed the behavior of statically determinate members, such as SSBs strengthened with FRP composites, few research studies have focused on the behavior of strengthened indeterminate members, such as continuous beams. Redistribution of the bending moment in ordinary continuous RC beams can be attributed to the structural redundancy and nonlinear behavior of RC. Such redistribution is affected by several factors, such as the quantity, arrangement, and mechanical characteristics of the internal steel; loading arrangement; geometry of the member; and the width and regions of the internal supports. Nonlinear analysis is an accurate approach for calculating the actual internal forces. However, existing building codes [39-41] allow us to take advantage of linear-elastic analysis with moment redistribution (15%–30%) for conventional structural designs. This means that the incorporation of moment redistribution in structural analysis is

reasonable and accurate to reduce the differences between the results of linear-elastic analysis and actual internal forces, which emerge as a result of the nonuniform stiffness distribution.

In ordinary indeterminate RC beams, the moment redistribution primarily depends on the amount of tension steel reinforcement ( $\rho_s$ ) in the bending moment regions. At the ultimate state, moment transfer occurs from the hogging region ( $h$ ) to the sagging region ( $s$ ) when  $\rho_s^h/\rho_s^s$  is not greater than 1.0, whereas when  $\rho_s^h/\rho_s^s$  is greater than 1.5 moment transfer occurs from the sagging region to the hogging region. However, when  $\rho_s^h/\rho_s^s$  lies between 1.0 and 1.5 the moment transfer is indistinct.

It should be noted that existing building codes [39-41] often tend to be conservative and do not allow moment redistribution for FRP strengthened structures, regardless of the amount of steel reinforcement at the critical sections. These codes prove that moment redistribution is a phenomenon that is mainly associated with flexural ductility, whereas FRPs are brittle materials. In addition, applying FRPs to strengthen and retrofit RC beams usually leads to nonconventional failure modes, such as IC debonding and peeling-off in the case of externally bonded laminates and pull-out in the case of internally bonded bars. These nonconventional failures may lead to a significant reduction in the beam's ductility state and its degree of moment redistribution ( $\beta$ ). However, despite being very limited in number, previous studies on EB-CFRP strengthened RC beams have indicated that moment redistribution is possible to some extent at the ultimate state, as shown in Table 5. In fact, moment redistribution is not only occurs at the ultimate state but also evolves throughout the whole loading process, even before the formation yielding of the tension steel reinforcement. According to the experimental results obtained from the tests performed in the present research, evolution of moment redistribution also seems to be significantly influenced depending on the strengthening state of the beam, as shown in Fig. 22.

In general, the degree of moment redistribution ( $\beta$ ) can be quantified using the values of flexural moments at the critical sections of a beam [45], as provided in Eq. 1, where  $M_{th}$  is the theoretical bending moment calculated on the basis of the linearly elastic statement and  $M_{exp}$  is the actual bending moment calculated from the experiment after moment redistribution:

$$\beta (\%) = \left( \frac{M^{Th} - M^{Exp}}{M^{Th}} \right) \times 100\% \quad (1)$$

Fig. 23 shows the experimental and elastic bending moments at the critical sections induced by the applied load, and the evolution of the moment ratio. The sagging bending moment ( $M_1$ ) is presented with a positive sign, and the hogging bending moment ( $M_2$ ) is presented with a negative sign. The experimental  $(M_1)_{exp}$  and  $(M_2)_{exp}$  values were calculated using Eqs. 2 and 3, respectively, and the elastic  $(M_1)_{el}$  and  $(M_2)_{el}$  values were calculated using Eqs. 4 and 5, respectively (see, Fig. 24). Overall, the experimental moments differed from the elastic ones, particularly after the concrete cracking load was reached. For all the tested beams, the elastic moment ratio  $(M_1/M_2)_{el}$  remained constant over the loading process, whereas the experimental moment ratio  $(M_1/M_2)_{exp}$  varied from one beam to another.

$$M_1^{Exp} = \frac{(P_u - R_c) \times L}{4} \quad (2)$$

$$M_2^{Exp} = \frac{(P_u - 2R_c) \times L}{4} \quad (3)$$

$$M_1^{Th} = \frac{5P_u L}{64} \quad (4)$$

$$M_2^{Th} = \frac{3P_u L}{32} \quad (5)$$

As can be seen in Fig. 23, the development of the actual moment ratio  $(M_1/M_2)_{exp}$  is strongly associated with the strengthening scenario applied. A decrease in  $(M_1/M_2)_{exp}$  indicates moment redistribution from the midspan toward the intermediate support, an increase in  $(M_1/M_2)_{exp}$  indicates moment redistribution from the intermediate support toward the midspan, and stabilization of  $(M_1/M_2)_{exp}$  indicates the stabilization of moment redistribution. It has also been shown that the majority of the moment redistribution, despite being limited, occurred in the stage between the concrete cracking and the first steel yielding. In this stage, the moment clearly transferred from the hogging region to the sagging region in beams BC1-EB1S, BC5-EB1S-*weight (700)*, and BC6-EB1S-*weight(1100)*, whereas it was pendulous about the elastic moment ratio  $(M_1/M_2)_{el}$  in beams BC2-EB1P and BC3-EB1S-*side*. The direction of moment transfer **was** totally changed when the number of CFRP sheets layers **was** increased. This can be observed in beam BC4-EB2S, in which the moment was transferred from the sagging region to the hogging region. However, after the yielding of the tension steel bars, slight moment redistribution occurred in all the beams, which **may** could be attributed to the fact that a similar amount of steel reinforcement was used in the beam's critical sections.

At the ultimate state, using EB-CFRP composites significantly decreased the moment redistribution degree ( $\beta$ ) of two-span continuous RC beams. The value of  $\beta$  for the control beam was +20.53% at the central support and -12.43% at the midspan. With regard to strengthened beams, beams BC1-EB1S, BC2-EB1P, BC3-EB1S-*side*, BC4-EB2S, BC5-EB1S-*weight(700)*, and BC6-EB1S-*weight(1100)* were found to have moment redistribution degrees of, respectively, +13.87%, +2.72%, +1.48%, -17.44%, +9.8%, and +6.1% at the central support, and -8.32%, -1.63%, -0.89%, +10.46%, -5.9%, and -3.7% at the midspan.

Table 5: Moment redistribution, as reported from literature, for continuous beams strengthened with EB-FRP at the ultimate state level.

Reference	Number of spans and dimensions <sup>(1)</sup>	Strengthening scenario	Failure mode	Mid-support $\beta$ (%)	Mid-span $\beta$ (%)
H. Akbarzadeh et al. [7]	Two-span beams 150×170×6000	Control beam	Flexural failure	16.06	-9.62
		EB-One sheet-CFRP in S and H <sup>(3)</sup>	rupture of top CFRP	8.22	-4.92
		EB-Two sheets-CFRP in S and H	IC debonding of FRP sheet and rupture of end strap at hogging region	3.57	-2.13
		EB-Three sheets-CFRP in S and H	IC debonding at hogging region	1.51	-0.71
		EB-Three sheets-GFRP in S and H	IC debonding at hogging region	3.81	-2.34
M. A. Aiello et al. [42]	Two-span beams 150×200×3500	Control beam	Flexural failure	-0.08	0.05
		EB-One sheet-CFRP in S		12.23	-8.82
		EB-One sheet-CFRP in S and H	Detaching of the FRP sheets together with concrete crushing	3.88	-2.78
		EB-Two sheets-CFRP in S		25.75	-18.57
		EB-One sheet-CFRP in H		-16.10	11.57
R. Feng et al. [43]	Two-span beams 150×250×2400	Control beam	Flexural failure	8.98	-5.37
		EB-Two layers of C-FRCM in S and H	Flexural failure and slippage of carbon fabric meshes within cementitious matrix	6.02	-3.63
		EB-Three layers of C-FRCM in S and H	Flexural failure, slippage of carbon fabric meshes within cementitious matrix, and debonding of C-FRCM from concrete substrate	5.45	-3.25
D.J. Oehlers et al. [44]	Two-span beams 375×120×5000	EB-One CFRP plate in H		35	N.A. <sup>(2)</sup>
		EB-One CFRP plate in H	CFRP plate debonding	36	N.A.
		EB-One CFRP plate in H		28	N.A.

(1) Beam dimension: width×depth×total length, all dimensions are in mm, (2) N.A. : data not available, (3) S: sagging region and H: hogging region.

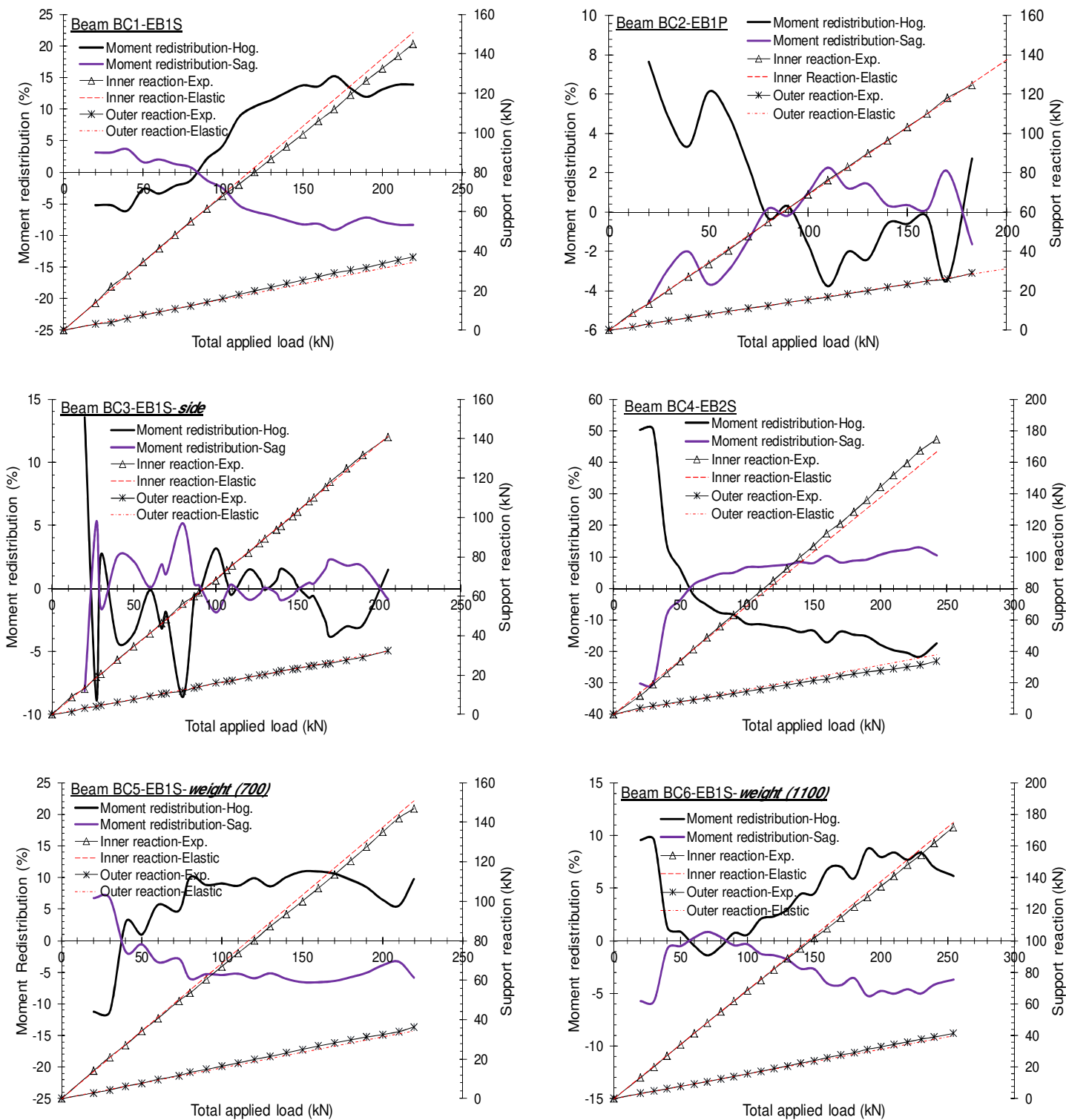
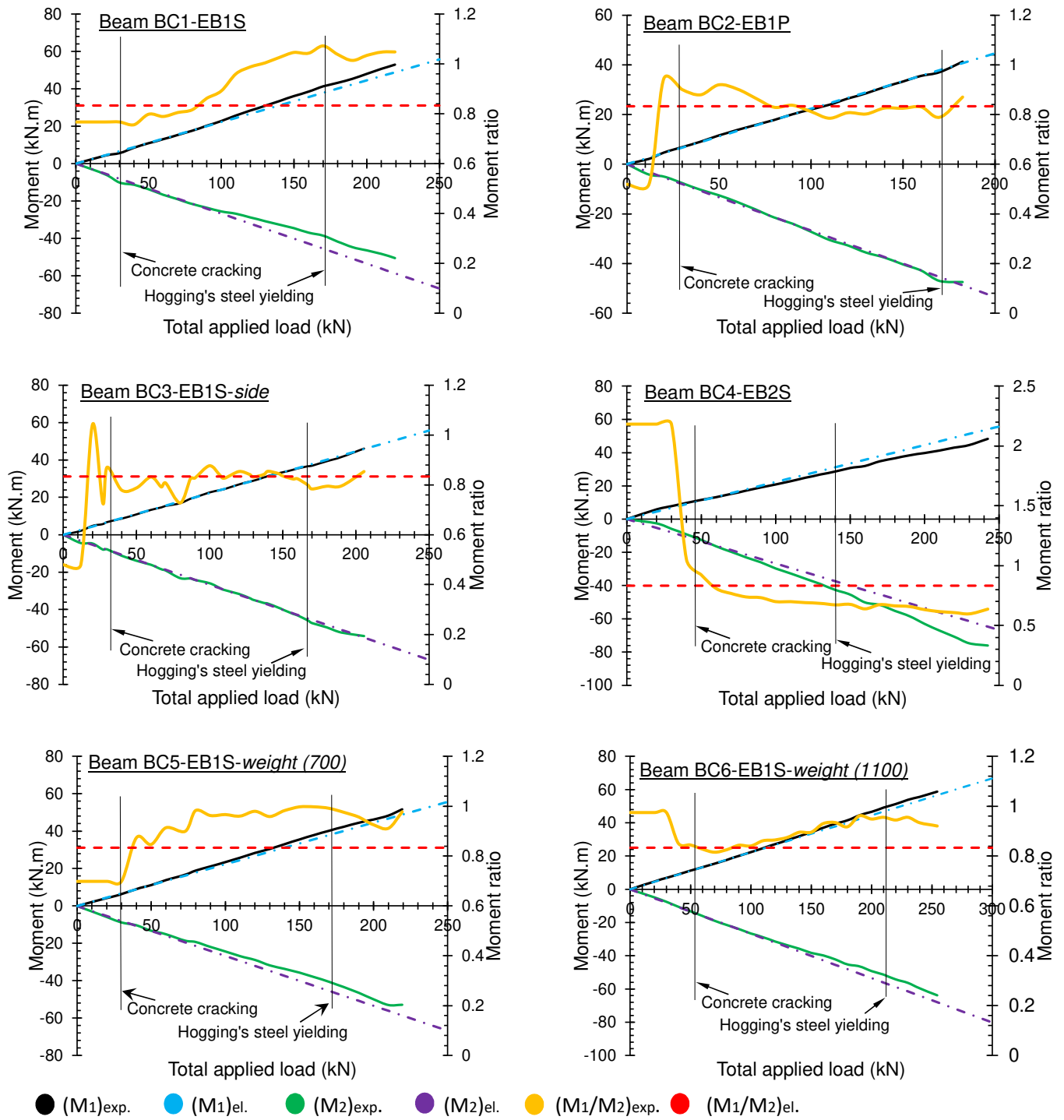


Fig. 22: Moment redistribution of tested strengthened beams





M1: Moment at sagging; and M2: Moment at hogging

Fig. 23: Moment ratio of tested strengthened beams

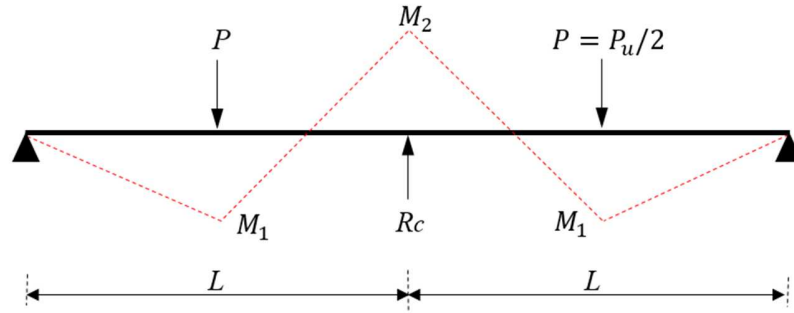


Fig. 24: Schematic drawing for loads and moments of tested beams.

### 3.2 Beams strengthened with NSM CFRP reinforcements

This section presents the main experimental results obtained from testing two continuous RC beams strengthened with NSM CFRP bars technique. In addition, it compares and assesses the effectiveness of the EB CFRP technique in strengthening continuous RC beam with respect to the NSM technique. To this end, the experimental results of the NSM beams (BC1-NSM and BC2-SNSM) were compared with the experimental results of EB beams (BC1-EB1S and BC3-EB1S-side) from the previous section (section 3.1).

#### 3.2.1 Overall performance

Table 6 presents a comparison between the main experimental results of the NSM beams and those of the EB beams in terms of the load-carrying capacity ( $P_u$ ), attained central reaction at the ultimate load level ( $R_c$ ), ultimate bending moment in the hogging ( $M_h^{Exp}$ ) and sagging ( $M_s^{Exp}$ ) regions, moment redistribution ratio ( $\beta$ ), ductility index ( $\mu$ ), and energy absorption capacity ( $E_{ab}$ ). The ductility index ( $\mu$ ) is defined as the ratio of deflection at the ultimate load to that at which the steel starts yielding. The energy absorption capacity ( $E_{ab}$ ) is calculated ~~on the basis of~~ from the area under the load-deflection curve up to the ultimate load.

In general, despite the smaller CFRP reinforcement area, continuous RC beams internally strengthened with CFRP rods exhibited a better flexural performance than that of beams strengthened externally with CFRP sheets. The same was also true regarding the ultimate strength capacity, moment redistribution capability, ductility state, and energy absorption capacity. This overall improvement is most likely attributed to the fact that the NSM-CFRP rods were located inside the strengthened members, providing an advanced level of strengthening that is less prone to premature failure and has high bonding efficiency. Indeed, according to the test results, the NSM technique showed a higher capability than that of the EB technique to delay the debonding failure. This can be clearly seen in Figs. 25 and 26, which present the variations in the longitudinal tensile strain of the CFRP under several load levels. It can also be observed that the debonding strain in beam BC1-NSM was 51.5% greater than that in beam BC1-EB1S and, similarly, 17.6% greater in beam BC2-SNSM than in beam BC3-EB1S-side.

Table 6: Comparison between the test results of the NSM/SNSM beams and EB beams

Beam	Ultimate load ( $P_u$ )	Central support reaction <sup>[1]</sup> $R_c$	Flexural moment at hogging ( $M_h$ )			Flexural moment at sagging ( $M_s$ )			$\mu$ <sup>[7]</sup>	$E_{ab}$ <sup>[8]</sup>
			$M_h^{Exp}$ <sup>[2]</sup>	$M_h^{Th}$ <sup>[3]</sup>	$\beta$ (%) <sup>[6]</sup>	$M_s^{Exp}$ <sup>[4]</sup>	$M_s^{Th}$ <sup>[5]</sup>	$\beta$ (%) <sup>[6]</sup>		
			CB	169.7	110.1	36	45.3	20.53		
BC1-NSM	277.1	180.3	59.5	74	19.59	69	61.7	-11.83	3.3	10356.6
BC2-SNSM	250.1	166.6	59.3	67	11.49	59.4	55.6	-6.92	3.6	11242.1
BC1-EB1S	219.4	145.1	50.5	58.6	13.87	52.9	48.9	-8.32	2.2	6044.3
BC3-EB1S- <i>side</i>	205.5	140.7	54.1	54.9	1.48	46.2	45.8	-0.89	2.8	6994.7

(1) Central reaction measured by attached load cell at ultimate load  $P_u$ . (Both in kN); (2) Experimental ultimate negative moment calculated by:  $M_h^{Exp} = \frac{(P_u - 2R_c) \times L}{4}$ , where L is the beam length. (kN.m); (3) Theoretical ultimate negative moment calculated by:  $M_h^{Th} = \frac{3P_u L}{32}$ . (kN.m); (4) Experimental ultimate positive moment calculated by:  $M_s^{Exp} = \frac{(P_u - R_c) \times L}{4}$ . (kN.m); (5) Theoretical ultimate positive moment calculated by:  $M_s^{Th} = \frac{5P_u L}{64}$ . (kN.m); (6) Moment redistribution calculated by:  $\beta$  (%) =  $\left( \frac{M^{Th} - M^{Exp}}{M^{Th}} \right) \times 100\%$ . ; (7) Ductility index.; (8) Energy absorption capacity. (kN.mm).

### 3.2.2 Failure mode and cracks maps

As stated in Section 3.1.2, the failure that occurred in the EB beams was primarily debonding of the CFRP sheets and plates at the critical sections as a result of the IC followed by either CCD or CFRP rupture. Table 7 presents the failure modes and crack maps of the NSM beams. The typical failure mode was yielding of the tension steel followed by debonding of the CFRP bars. No delamination of the concrete cover or rupture of the CFRP bars was observed. Notably, the debonding failure of beam BC1-NSM was brittle as a consequence of the sudden pulling-out of the CFRP bars in the hogging region close to the central support, accompanied by **with** minor concrete crushing at the applied load points. The debonding failure of beam BC2-SNSM was characterized by the cracking of the epoxy-resin cover and the fracture in the concrete at the hogging and sagging regions, with high-intensity concrete crushing at the applied load points and minor concrete crushing at the central support. It was also found that, in each beam, one end of the CFRP bars moved from its initial position to the central support, indicating that the debonding failure primarily occurred at the resin-CFRP interface, not as a result of the IC. This finding confirms that the NSM-CFRP bars in continuous RC beams are less sensitive to debonding phenomena due to the IC, which is similar to the results observed in SSBs [24].

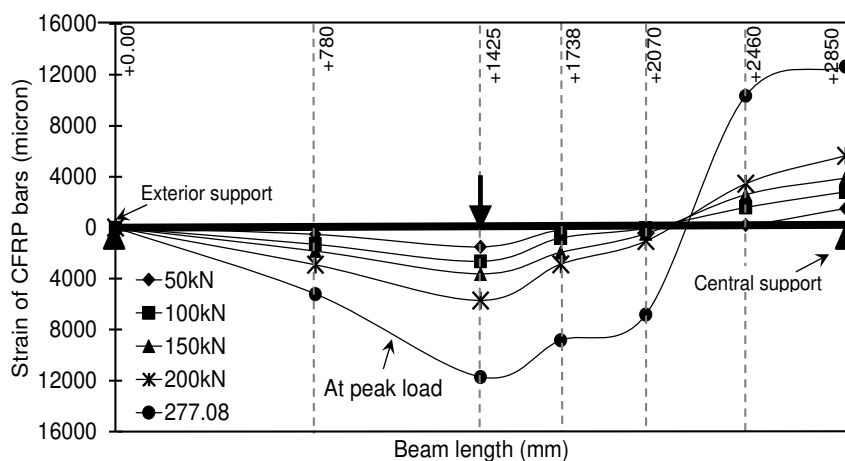
The number of cracks at the failure stage was also found to be lower in the EB beams than that reported in the NSM beams, especially in the hogging region. Compared to the control beam, the number of cracks in beam BC1-NSM was higher by 200% (189% for BC1-EB1S) and 62.5% (125% for beam BC1-EB1S) in the hogging and sagging regions, respectively, whereas the number of cracks in beam BC2-SNSM was higher by 250% (63% for beam BC3-EB1S-*side*) in the hogging region and 193.8% (19% for BC3-EB1S-*side*) in the sagging region.

### 3.2.3 Yield and ultimate strength capacity

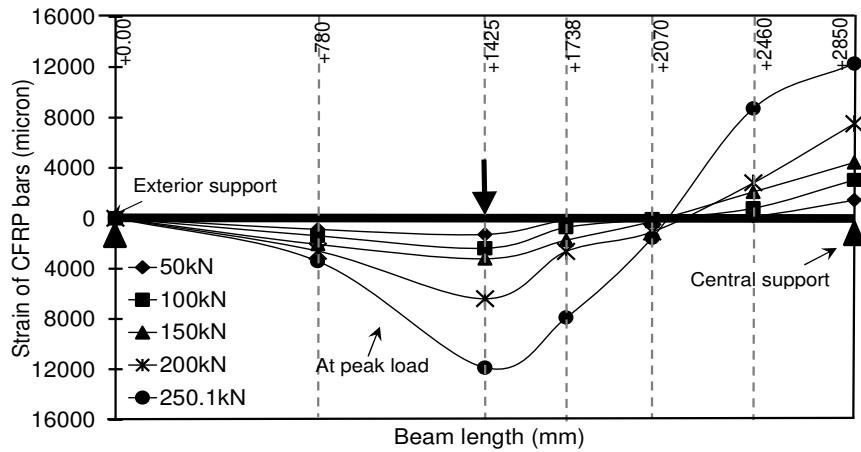
Although the axial stiffness ratios of beams BC1-NSM, BC2-SNSM, BC1-EB1S, and BC3-EB1S-*side* were very close, the amount of CFRP reinforcement used to strengthen the EB beams

(BC1-EB1S, BC3-EB1S-side) was nearly 1.27 times that used to strengthen the NSM beams (BC1-NSM, BC2-SNSM). According to Fig. 27, the tested beams, regardless of the strengthening technique used, displayed an almost similar identical response in the elastic stage (i.e. before the concrete cracking). In the postcracking and postyielding stages, however, the flexural stiffness, yielding load, and ultimate load of the NSM beams were considerably higher than those of the EB beams. The tension steel in the hogging region of beams BC1-NSM and BC2-SNSM yielded at a load of 195.1kN (13.8% increase over BC1-EB1S) and 180.8 kN (8.9% increase over BC3-EB1S-side), respectively. Similarly, the ultimate strength capacity of beams BC1-NSM and BC2-SNSM was about 277.1 kN (26.3% increase over BC1-EB1S) and 250.1 kN (21.8% increase over BC3-EB1S-side), respectively. These results indicate that improving the flexural behavior of continuous RC beams is more dependent on the strengthening technique used than on the CFRP reinforcement amount or axial stiffness ratio applied. This was also true regarding beam BC4-EB2S (see Fig. 18), in which the area of the CFRP sheets (two layers) was nearly 2.5 times that used to strengthen beam BC1-NSM (2 $\phi$ 6). Moreover, the yielding and ultimate capacity of the latter beam (BC1-NSM) were still greater by about 2.7% and 14.3%, respectively. Therefore, it was confirmed that the NSM technique is more efficient than the EB technique.

In general, positioning the CFRP reinforcements on the vertical sides instead of the bottom/top sides decreases the effective arm depth of the tension reinforcements, thereby decreasing the yield and ultimate strength of the beam. In this study, the reduction in the ultimate strength due to changing the position of the CFRP was marginally affected by the strengthening technique used. The percentage drops of the ultimate strength for beams strengthened with EB sheets and NSM-CFRP rods were 6.4% and 9.7%, respectively. In SSBs, however, this percentage drop was 16.1% in the EB-CFRP beams [10] and 12.9% in the NSM-CFRP beams [11].

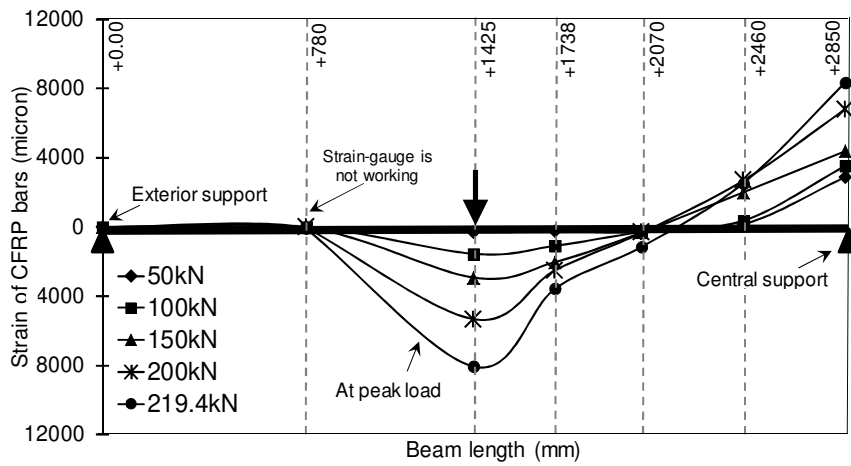


(a) BC1-NSM

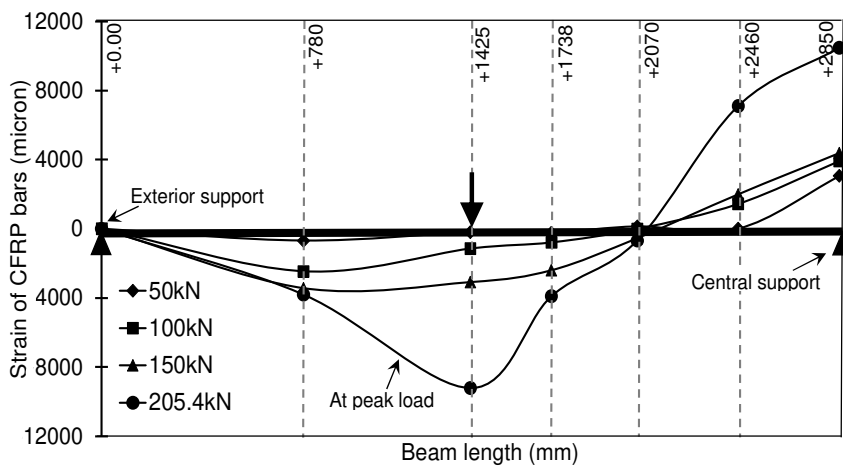


(b) BC2-SNSM

Fig. 25: Variation in longitudinal strain of NSM-CFRP bars at different loads



(a) BC1-EB1S



(b) BC3-EB1S-side

Fig. 26: Variation in longitudinal strain of EB-CFRP bars at different loads.

### 3.2.4 Moment redistribution

As discussed previously in [Section 3.1.5](#), strengthening continuous RC beams with EB-CFRP sheets significantly decreases the moment redistribution degree at the ultimate state and can even change the direction of redistribution depending on the strengthening state. However, by comparing the moment redistribution values of beams BC1-NSM and BC2-SNSM with those of the RC beam strengthened with EB-CFRP sheets (BC1-EB1S, BC3-EB1S-side), it can be concluded that applying the NSM technique allows a higher moment redistribution value at the ultimate state, as shown in [Table 6](#). Further research studies are strongly recommended in this direction.

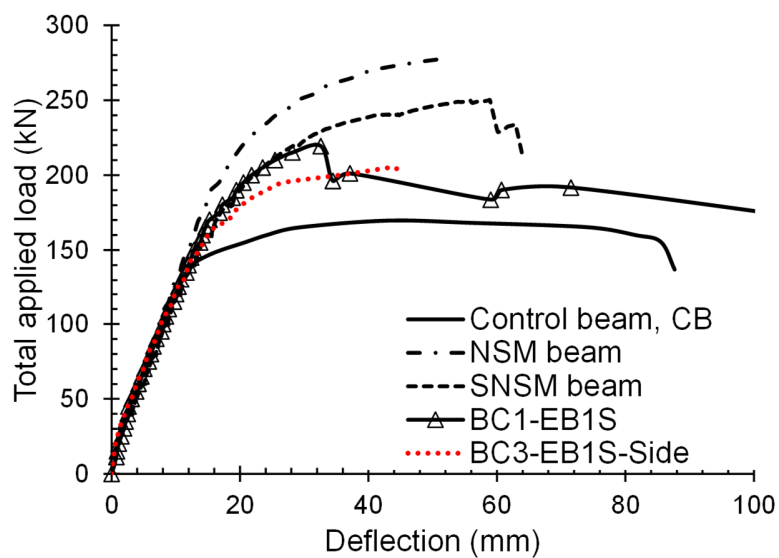



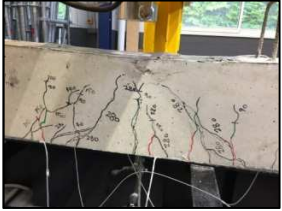
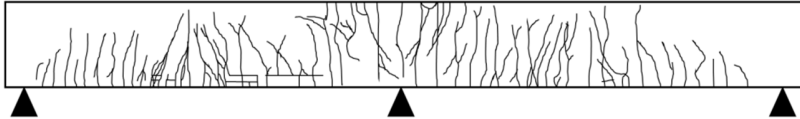





Fig. 27: Load deflection curves of NSM/SNSM beams and EB beams

Table 7: Crack maps and failure mode of the NSM beams

Beam	Cracks map	Failure mode		
BC1-NSM				
Debonding: Pull out of the CFRP bars in the hogging region				
BC2-SNSM				
Debonding: Cracking of the epoxy-resin cover and fracture in the concrete in the hogging and sagging regions				

#### 4. Evaluation of the effectiveness of the current guidelines in determining the flexural strength of EB-CFRP continuous beams

In this section, three analytical models for the estimation of the flexural capacity of RC beams strengthened with EB-CFRP sheets/plates are analyzed. The experimental ultimate bending moments of EB-CFRP beams were compared with the design ultimate bending moments computed using the formula provided in the American ACI 440.2R-08 [30], Italian CNR-DT 200 R1/2013 [37], and technical report of FIB Bulletin 14 [38]. Notably, the compressive strength of concrete cylinders ( $f'_c$ ) is normally used in these guidelines, which is determined in the laboratory in this study. It is important to note that the ultimate compressive strain of concrete ( $\varepsilon_{cu}$ ) defined in the aforementioned design guidelines is different. In ACI 440.2R-08 [30],  $\varepsilon_{cu}$  is defined as 0.003, whereas it is defined as 0.0035 in CNR-DT 200 R1/2013 [37] and FIB Bulletin 14 [38]. These three guidelines include the same procedure for calculating the depth of the neutral axis based on the strain compatibility and internal forces equilibrium. However, they feature different assumptions regarding the effective strain of EB-FRP composites, as will be discussed in detail in the following sections. The steel reinforcement used was elasto-plastic with an elastic modulus of 192.85 GPa, and the material behavior of the CFRP reinforcement was linearly elastic until failure, which is defined by the manufacturer and the current design guidelines.

##### 4.1 ACI 440.2R-08 [30]

According to the ACI 440.2R-08 guideline, the tensile strain of the external CFRP composite should be limited to the debonding strain  $\varepsilon_{fd}$ , as provided in Eq. 6, where;  $f'_c$  is the compressive strength of concrete;  $n$ ,  $E_f$ , and  $t_f$  are the number of layers, modulus of elasticity, and thickness of the CFRP, respectively; and  $\varepsilon_{fu} = C_E \varepsilon_{fu}^*$  is the design rupture strain, which is calculated by considering reduction for environmental exposure condition. In this study, an environmental reduction factor ( $C_E$ ) of 0.95 is considered.

$$\varepsilon_{fd} = 0.41 \sqrt{\frac{f'_c}{nE_f t_f}} \leq 0.9\varepsilon_{fu} \quad (6)$$

The effective level of strain in the CFRP ( $\varepsilon_{ef}$ ), concrete ( $\varepsilon_c$ ), tension steel ( $\varepsilon_s$ ), and compression steel ( $\varepsilon'_s$ ) can be estimated using the following strain compatibility equations:

$$\varepsilon_{ef} = \varepsilon_{cu} \left( \frac{d_f - c}{c} \right) \leq \varepsilon_{fd} \quad (7)$$

$$\varepsilon_c = \varepsilon_{ef} \left( \frac{c}{d_f - c} \right) \quad (8)$$

$$\varepsilon_s = \varepsilon_{ef} \left( \frac{d - c}{d_f - c} \right) \quad (9)$$



$$\varepsilon'_s = \varepsilon_{ef} \left( \frac{c - d'}{d_f - c} \right) \quad (10)$$

where  $c$  is the depth of the neutral axis, which is calculated using the internal force equilibrium:

$$\alpha_1 \beta_1 f'_c b c + A'_s f'_s = A_s f_s + A_f f_{fe} \quad (11)$$

where  $\alpha_1$  (Eq. 12) and  $\beta_1$  (Eq. 13) are the concrete stress block factors, and  $\varepsilon'_c$  (Eq. 14) is the compressive strain of unconfined concrete. Hence,

$$\alpha_1 = \frac{3\varepsilon'_c(\varepsilon_c - \varepsilon_c^2)}{3\beta_1 \varepsilon_c'^2} \quad (12)$$

$$\beta_1 = \frac{4\varepsilon'_c - \varepsilon_c}{6\varepsilon'_c - 2\varepsilon_c} \quad (13)$$

$$\varepsilon'_c = \frac{1.7f'_c}{E_c} \quad (14)$$

~~Following the above indications,~~ The flexural strength of the strengthened section ( $M_n$ ) can be calculated as provided in Eqs. 15-17. In these equations,  $M_{ns}$  and  $M_{nf}$  are the steel and CFRP contribution to bending, respectively;  $\phi$  and  $\psi_f$  are the strength reduction factor ( $\phi = 0.9$ ) and additional recommended reduction factor ( $\psi_f = 0.85$ ) on the flexural strength contribution of the CFRP reinforcement, respectively;  $A_s$  and  $A_f$  are the areas of the tension steel and CFRP, respectively; and  $d$  and  $d_f$  are the effective depths of steel and CFRP, respectively. Hence,

$$\phi M_n = \phi [M_{ns} + \psi_f M_{nf}] \quad (15)$$

$$M_{ns} = A_s f_s \left( d - \frac{\beta_1 c}{2} \right) \quad (16)$$

$$M_{nf} = A_f f_{fe} \left( d_f - \frac{\beta_1 c}{2} \right) \quad (17)$$

#### 4.2. CNR-DT 200 R1/2013 [37]

According to the Italian CNR-DT 200 R1/2013 guideline, the tensile strain of the external CFRP composite should be limited to  $\varepsilon_{fd}$ , as provided in Eq. 18, where  $n_a$  (0.85) is the environmental conversion factor,  $\gamma_f$  is the material safety factor (1.1 for the ultimate limit state),  $\varepsilon_{fk} = \frac{f_{fk}}{E_f}$  is the CFRP characteristic failure strain, and  $\varepsilon_{fdd}$  is the CFRP IC-induced debonding strain. Hence,

$$\varepsilon_{fd} = \min \left[ \frac{n_a \varepsilon_{fk}}{\gamma_f}, \varepsilon_{fdd} \right] \quad (18)$$

The CFRP IC-induced debonding strain can be determined as follows:

$$\varepsilon_{fdd} = \frac{k_q}{\gamma_{f,d}} \sqrt{\frac{2k_b k_{G2}}{t_f E_f FC} \sqrt{f_{cm} \cdot f_{ctm}}} \geq \varepsilon_{sy} - \varepsilon_0 \quad (19)$$

where  $k_q$  is a coefficient that considers load distribution and is equal to 1.25 for distributed loads and 1.0 for all other load configurations;  $\gamma_{f,d}$  is a safety factor that depends on the probability associated with debonding failure, which can be chosen by the designer in the range between 1.20 and 1.50; FC is a calibrated factor of confidence related to the level of knowledge of the element to be strengthened;  $k_{G2}$  is a corrective factor calibrated on the experimental results and is equal to 0.10 mm irrespective of the type of reinforcement;  $f_{cm}$  and  $f_{ctm}$  are the concrete mean compressive and tensile strength, respectively;  $\varepsilon_{sy}$  is the design yield strain of the steel reinforcement;  $\varepsilon_0$  is the maximum tensile strain present before the FRP is applied; and  $k_b$  (Eq. 20) is the geometrical corrective factor, which is a function of the ratio between the CFRP and the concrete width ( $b_f/b$ ):

$$k_b = \sqrt{\frac{2-b_f/b}{1+b_f/b}} \geq 1 \text{ for } b_f/b \geq 0.25 \quad (20)$$

For a bond length ( $l_b$ ) shorter than the design optimal bond length ( $l_{ed}$ ), the debonding strain ( $\varepsilon_{fad}$ ) should be reduced to the plate-end debonding strain as follows:

$$\varepsilon_{fdd} = \frac{k_q}{\gamma_{f,d}} \sqrt{\frac{2k_b k_{G2}}{t_f E_f FC} \sqrt{f_{cm} \cdot f_{ctm}}} \cdot \frac{l_b}{l_{ed}} \left(2 - \frac{l_b}{l_{ed}}\right) \geq \varepsilon_{sy} - \varepsilon_0 \quad (21)$$

where

$$l_{ed} = \min\left[\frac{1}{\gamma_{Rd}} \sqrt{\frac{\pi^2 t_f E_f S_u^2 FC}{8k_b k_{G2} \sqrt{f_{cm} \cdot f_{ctm}}}}, 200\text{mm}\right] \quad (22)$$

In which  $S_u$  is the FRP-concrete interfacial debonding slip and  $\gamma_{Rd}$  is the partial factor for resistance models (assuming  $\gamma_{Rd} = 1$  in this study).

However, the CNR-DT 200 R1/2013 guideline classifies the failure mode of the strengthened section into two categories: (i) failure due to concrete crushing if  $\mu_f > \mu_{f1-2}$  and (ii) failure due to rupture of the FRP if  $\mu_f < \mu_{f1-2}$ , in which  $\mu_f$  and  $\mu_{f1-2}$  are defined in Eq. 23 and Eq. 24, respectively. In the case of failure due to concrete crushing, the effective strain in the CFRP ( $\varepsilon_f$ ), concrete ( $\varepsilon_c$ ), tension steel ( $\varepsilon_{s1}$ ), and compression steel ( $\varepsilon_{s2}$ ) can be obtained from Eq. 25. In the case of failure due to rupture of the FRP, the effective strain in the materials can be obtained from Eq. 26.

$$\mu_f = \frac{b_f (n_f t_f) f_{dd,2}}{f_{cd} b d} \quad (23)$$

$$\mu_{f1-2} = \frac{0.8\varepsilon_{cu}h/d}{\varepsilon_{cu} + \varepsilon_{fd} + \varepsilon_0} - \mu_s(1 - u) \quad (24)$$

$$\left\{ \begin{array}{l} \text{CFRP} \\ \text{Concrete} \\ \text{Tension steel} \\ \text{Compression steel} \end{array} \right. \quad \left\{ \begin{array}{l} \varepsilon_f = \frac{\varepsilon_{cu}}{x}(h - x) - \varepsilon_0 \leq \varepsilon_{fd} \\ \varepsilon_c = \varepsilon_{cu} \\ \varepsilon_{s1} = \varepsilon_{cu} \frac{d - x}{x} \\ \varepsilon_{s2} = \varepsilon_{cu} \frac{x - d_2}{x} \end{array} \right. \quad (25)$$

$$\left\{ \begin{array}{l} \text{CFRP} \\ \text{Concrete} \\ \text{Tension steel} \\ \text{Compression steel} \end{array} \right. \quad \left\{ \begin{array}{l} \varepsilon_f = \varepsilon_{fd} \\ \varepsilon_c = (\varepsilon_{fd} + \varepsilon_0) \frac{x}{h - x} \leq \varepsilon_{cu} \\ \varepsilon_{s1} = (\varepsilon_{fd} + \varepsilon_0) \frac{d - x}{h - x} \\ \varepsilon_{s2} = (\varepsilon_{fd} + \varepsilon_0) \frac{x - d_2}{h - x} \end{array} \right. \quad (26)$$

~~Following the above indications,~~ The flexural strength of the strengthened section ( $M_{Rd}$ ) can be calculated as follows:

$$M_{Rd} = \frac{1}{\gamma_{Rd}} [\psi b x f_{cd} (d - \lambda x) + A_{s2} \sigma_{s2} (d - d_2) + A_f \sigma_f d_1] \quad (27)$$

where  $\psi$  and  $\lambda$  are nondimensional coefficients representing the intensity and position of the compressive concrete resultant, respectively;  $f_{cd}$  is the design concrete compressive strength;  $d$ ,  $d_1$  and  $d_2$  are the effective depths of the tension steel, CFRP, and compression steel, respectively;  $\sigma_{s2}$  is the stress in the compression steel;  $\sigma_f$  is the stress in the CFRP;  $A_{s2}$  and  $A_f$  are the areas of the compression steel and CFRP, respectively; and  $x$  is the depth of the neutral axis, calculated as in the following equation:

$$0 = \psi b x f_{cd} + A_{s2} \sigma_{s2} - A_{s1} \sigma_{s1} - A_f \sigma_f \quad (28)$$

#### 4.3 ~~FIB~~ fib Bulletin 14 [38]

Although the technical report of ~~FIB~~ fib Bulletin 14 provides a formula (Eq. 29) for limiting stress in the FRP composite in the service limit state, it does not provide a specific formula for reducing the strain of the external CFRP composite during analysis in the ultimate limit state. The only check provided in the ultimate limit state so far is the straining of the FRP ( $\varepsilon_f$ ) not exceeding the ultimate strain ( $\varepsilon_{fud}$ ) when a conventional failure occurs. The design bending moment of the strengthened cross section (Eq. 30) is calculated on the basis of the general principles of the RC design [36]. The neutral axis depth ( $x$ ) is calculated from the strain

compatibility and internal force equilibrium, and the design moment is obtained from the moment equilibrium:

$$\sigma_{FRP} = E_f \left( \varepsilon_c \frac{h - X_e}{X_e} - \varepsilon_0 \right) \leq \eta f_{fk} \quad (29)$$

where  $X_e$  is the neutral axis depth;  $\eta$  is the FRP stress limitation coefficient, which depends on the type of FRP and should be obtained through experiments; the suggested  $\eta$  value for the CFRP is 0.8; and  $f_{fk}$  is the characteristic value of the FRP tensile strength:

$$M_{Rd} = A_{s1} f_{yd} (d - \delta_G x) + A_f E_f \varepsilon_f (h - \delta_G x) + A_{s2} E_s \varepsilon_{s2} (\delta_G x - d_2) \quad (30)$$

where  $\delta_G = 0.4$  is the coefficient of the rectangular stress centroid for concrete in compression and  $x$  is the depth of the neutral axis, which is calculated as follows:

$$0.85 \psi f_{cd} b x + A_{s2} E_s \varepsilon_{s2} = A_{s1} f_{yd} + A_f E_f \varepsilon_f \quad (31)$$

In Eq. 31,  $\psi = 0.8$  is the coefficient of the rectangular stress area for concrete in compression.

It is worth noting that, in the case of failure due to the FRP reinforcements, **FIB** *fib* Bulletin 14 [34] provides modifications for the values of  $\delta_G$  and  $\psi$  as follows:

$$\psi = \begin{cases} 100 \varepsilon_c \left( 0.5 - \frac{1000}{12} \varepsilon_c \right) & \text{for } \varepsilon_c \leq 0.002 \\ 1 - \frac{2}{3000 \varepsilon_c} & \text{for } 0.002 \leq \varepsilon_c \leq 0.0035 \end{cases} \quad (32)$$

$$\delta_G = \begin{cases} \frac{8 - 1000 \varepsilon_c}{4(6 - 1000 \varepsilon_c)} & \text{for } \varepsilon_c \leq 0.002 \\ \frac{1000 \varepsilon_c (3000 \varepsilon_c - 4) + 2}{2000 \varepsilon_c (3000 \varepsilon_c - 2)} & \text{for } 0.002 \leq \varepsilon_c \leq 0.0035 \end{cases} \quad (33)$$

#### 4.4. Comparison of the ultimate bending moment obtained from tests and current design codes

The experimental ultimate bending moments of the EB-CFRP beams were compared with the design ultimate bending moments obtained from the American ACI 440.2R-08 [30], Italian CNR-DT 200 R1/2013 [37], and technical report of **FIB** *fib* Bulletin 14 [38]. Comparisons regarding are listed in Table 8. It is worth noting that the design formulas provided in these codes do not include the mechanical properties of adhesive resin materials, however, they generally provide an acceptable prediction of the beam's flexural strength. The main observation pertained to the prediction accuracy for the flexural strength of multi-layer CFRP sheet beams, which was low and did not reflect the actual value. However, the mean values of the design-to-experimental bending moment ratios ( $M_{ACI}/M_{Exp}$ ,  $M_{CNR}/M_{Exp}$ , and  $M_{FIB}/M_{Exp}$ ) were found to be, respectively, 0.89, 0.88, and 1.06 in the hogging region and 1.01, 0.97, and 1.21 in the sagging region. Therefore, it can be concluded that the American ACI 440.2R-08 [30] and Italian CNR-

DT 200 R1/2013 [37] are relatively more conservative and appropriate than the technical report of ~~FIB~~ *fib* Bulletin 14 [38] in terms of predicting the flexural strength of RC continuous beams strengthened with EB-CFRP.

Table 8: Comparison of the ultimate bending moment obtained from the tests and current design codes.

Specimen	Experimental ultimate bending moment, $M_{exp}$ (kN.m)		ACI 440.2R-08 [30]	CNR-DT 200 R1/2013[37]	FIB fib Bulletin 14[38]			
	Hogging ( $h$ )	Sagging ( $s$ )	$M_{ACI}$ (kN.m)	$M_{CNR}$ (kN.m)	$M_{FIB}$ (kN.m)	$M_{ACI}/M_{Exp}$	$M_{CNR}/M_{Exp}$	$M_{FIB}/M_{Exp}$
CB	36	42.5	----	----	----	----	----	----
BC1-EB1S	50.5	52.9	48.87	48.90	53.9	0.97( $h$ ) 0.92( $s$ )	0.97( $h$ ) 0.92( $s$ )	1.07( $h$ ) 1.02( $s$ )
BC2-EB1P	47.4	41.3	41.49	40.10	57.26	0.88( $h$ ) 1.00( $s$ )	0.85( $h$ ) 0.97( $s$ )	1.21( $h$ ) 1.39( $s$ )
BC3-EB1S- <i>side</i>	54.1	46.2	46.14	47.54	50.94	0.85( $h$ ) 1.00( $s$ )	0.87( $h$ ) 1.03( $s$ )	0.94( $h$ ) 1.10( $s$ )
BC4-EB2S	76.1	48.3	55.64	51.90	66.16	0.73( $h$ ) 1.15( $s$ )	0.68( $h$ ) 1.07( $s$ )	0.87( $h$ ) 1.37( $s$ )
BC5-EB1S- <i>weight(700)</i>	52.9	51.7	51.75	51.45	59.06	0.98( $h$ ) 1.00( $s$ )	0.97( $h$ ) 0.99( $s$ )	1.12( $h$ ) 1.14( $s$ )
BC6-EB1S- <i>weight(1100)</i>	63.82	58.76	58.88	58.74	71.84	0.92( $h$ ) 1.00( $s$ )	0.92( $h$ ) 1.00( $s$ )	1.13( $h$ ) 1.22( $s$ )
Mean						0.89( $h$ ) 1.01( $s$ )	0.88( $h$ ) 0.97( $s$ )	1.06( $h$ ) 1.21( $s$ )

## 5. Conclusion

In this study, a total of nine beams were experimentally tested (i) to primarily investigate the effectiveness of the EB technique in improving the flexural performance of two-span RC beams in terms of important influential factors, such as the position, form, and reinforcement ratio of the CFRP, as well as the weight of carbon fibers; (ii) to evaluate the effectiveness of the current guidelines in determining the flexural strength of continuous RC beams strengthened externally with CFRP; and (iii) to assess and compare the efficiency of the EB technique in strengthening continuous beams to that of the NSM technique.

Regarding the effectiveness of the EB technique in improving the flexural performance of two-span RC beams, the following conclusions can be drawn:

- 1) Regardless of the strengthening scenario applied, all the strengthened beams displayed an improvement in their flexural strength in comparison to the unstrengthened control beam. ~~Such an~~ The increased ~~d~~ in the percentage of the yield and ultimate load as a result of the CFRP composites ranged from 25.5% to 59.1% and from 7.6% to 49.8%, respectively.
- 2) Increasing the carbon fiber weight per unit area was found to be effective in improving the strength capacity of the beam and it may be used as an alternative to multiple sheet layers, but this efficiency was conditional upon the total axial stiffness ratio of the beam and the proper adhesive resin used. The failure load of beam BC5-EB1S (one sheet, weight: 700 g/m<sup>2</sup>, axial stiffness: 1.17, Epx TFC 350) was found to be 99.2% of the total failure load of beam BC1-EB1S (one sheet, weight: 350 g/m<sup>2</sup>, axial stiffness =1.13, Epx TFC 350), whereas the failure load of beam BC6-EB1S (one sheet, weight: 1100 g/m<sup>2</sup>, axial stiffness =1.33, Epx TFC 1000) was found to be 116% of the failure load of beam BC1-EB1S. ~~104.9% of the total failure load of beam BC4-EB2S (two sheets, 350 g/m<sup>2</sup>)~~
- 3) Bonding the CFRP sheet on the side surfaces may be a feasible alternative to bonding on the bottom/top surfaces. Compared to beam BC1-EB1S, the decreases observed in the yield and ultimate load of beam BC3-EB1S-*side* were only 3.1% and 6.4%, respectively.
- 4) Moment redistribution analysis showed that the majority of moment redistribution occurred in the stage between the concrete cracking and the first steel yielding for all the tested beams, while slight moment redistribution occurred during later stages ~~after that~~.

Regarding the comparison between the two strengthening techniques, NSM and EB, the following conclusions can be drawn:

- 1) The NSM technique allows the CFRP tensile strength to be better exploited than the EB technique. The debonding strain in beam BC1-NSM was found to be 51.5% greater than that in beam BC1-EBIS and was also 17.6% greater in beam BC2-SNSM than in beam BC3-EBIS-*side*.

- 2) The flexural stiffness, yielding load, ultimate load, ductility state, and energy absorption capacity of the NSM beams were found to be considerably higher than those of the EB beams, confirming the higher efficiency of the NSM technique in comparison to the EB technique.
- 3) The NSM-CFRP bars in continuous RC beams were found to be less sensitive to debonding phenomena caused by the IC, which is not the case in EB-CFRP. The failure of the EB beams was characterized by debonding of the CFRP composites at the critical sections as a result of the IC followed by either CCD or CFRP rupture.
- 4) The NSM technique allows a higher moment redistribution value at the ultimate state than that achieved with the EB technique. Beams BC1-NSM and BC2-SNSM were found to exhibit moment redistribution degree of +19.59% and +11.49% in the hogging region and -11.83% and -6.92% in the sagging region, respectively, whereas their counterpart EB beams exhibited values of +13.87% and +1.48% in the hogging region and -8.32% and -0.89% in the sagging region.

Regarding the evaluation of the effectiveness of the current guidelines in determining the flexural strength capacity of continuous RC beams strengthened externally with CFRP, the following conclusion can be drawn:

The current design guidelines provide an acceptable prediction regarding the ultimate strength of beams strengthened with one layer of CFRP composites, however, **whereas** they show a low accuracy in predicting the ultimate strength for beams strengthened with multiple CFRP layers.

### **Acknowledgement**

The authors acknowledge the financial support of the Freyssinet Company, France.



## References

1. W.K. Goertzen, M.R. Kessler. Creep behavior of carbon fiber/epoxy matrix composites. *Materials Science and Engineering A* 421 (2006) 217–225.
2. A.N. Nayak, A. Kumaria , R.B. Swainb. Strengthening of RC Beams Using Externally Bonded Fibre Reinforced Polymer Composites Structures 2018;14: 137–152.
3. F. Al-Mahmoud, A. Castel, R. François, C. Tourneur. Strengthening of RC members with near-surface mounted CFRP rods. *Composite Structures* 2009; 91:138-147.
4. F. Al-Mahmoud , A. Castel , R. François , C. Tourneur . Effect of surface preconditioning on bond of carbon fiber reinforced polymer rods to concrete. *Cem.Concr. Compos.* 2007;29(9):677–89.
5. F. Ceroni, M. Pecce, A. Bilotta, E. Nigro. Bond behavior of FRP NSM systems in concrete elements . *Composites: Part B* 43 (2012) 99–109.
6. AF Ashour, SA El-Refaie, SW Garrity. Flexural strengthening of RC continuous beams using CFRP laminates. *Cem Concr Compos* 2004;26:765–75.
7. H Akbarzadeh, AA Maghsoudi. Experimental and analytical investigation of reinforced high strength concrete continuous beams strengthened with fiber reinforced polymer. *Mater Des* 2010;31:1130–47.
8. H. Ali, J. Assih, A. Li. Flexural capacity of continuous reinforced concrete beams strengthened or repaired by CFRP/GFRP sheets. *International Journal of Adhesion and Adhesives* 104 (2021) 102759.
9. M. Abdallah , F. Al Mahmoud, A. Khelil, J. Mercier, B. Almassri. Assessment of the flexural behavior of continuous RC beams strengthened with NSM-FRP bars, experimental and analytical study, *Composite Structures*, 242 (2020) 112127. <https://doi.org/10.1016/j.compstruct.2020.112127>.
10. A.S.D. Salama, R.A. Hawileh, J.A. Abdalla. Performance of externally strengthened RC beams with side-bonded CFRP sheets. *Composite Structures* 212 (2019) 281–290.
11. M. Abdallah, F. Al Mahmoud , R. Boissière , A. Khelil , J. Mercier. Experimental study on strengthening of RC beams with Side Near Surface Mounted technique-CFRP bars. *Composite Structures* 234 (2020) 111716. <https://doi.org/10.1016/j.compstruct.2019.111716>.
12. R. Capozucca, M. Nilde Cerri. Static and dynamic behaviour of RC beam model strengthened by CFRP-sheets. *Construction and Building Materials* 16 2002 91 Ž . 99.
13. Chao-Yang Zhou, Ya-Nan Yu, En-Li Xie. Strengthening RC beams using externally bonded CFRP sheets with end selflocking. *Composite Structures* 241 (2020) 112070.
14. A.N. Ababneh , R.Z. Al-Rousan, I.M.N. Ghaith. Experimental study on anchoring of FRP-strengthened concrete beams. *Structures* 23 (2020) 26–33.
15. I.A. Sharaky, M. Baena, C. Barris, H.E.M. Sallam, L. Torres. Effect of axial stiffness of NSM FRP reinforcement and concrete cover confinement on flexural behaviour of strengthened RC beams: Experimental and numerical study. *Engineering Structures* 173 (2018), 987–1001. <https://doi.org/10.1016/j.engstruct.2018.07.062>.
16. K. Le-Trung , K. Lee, J. Lee, D. H. Lee, S. Woo . Experimental study of RC beam–column joints strengthened using CFRP composites. *Composites: Part B* 41 (2010) 76–85.
17. A. Jawdhari , A. Peiris , I. Harika. Experimental study on RC beams strengthened with CFRP rod panels. *Engineering Structures* 173 (2018) 693–705.

18. Y. T. Obaidat , G.A.F.R. Abu-Farsakh , A. M. Ashteyat. Retrofitting of partially damaged reinforced concrete beam-column joints using various plate-configurations of CFRP under cyclic loading. *Construction and Building Materials* 198 (2019) 313–322.
19. A. Akhlaghi , D. Mostofinejad. Experimental and analytical assessment of different anchorage systems used for CFRP flexurally retrofitted exterior RC beam-column connections. *Structures* 28 (2020) 881–893.
20. GP. Lignola, A. Prota, G. Manfredi, E. Cosenza. Experimental performance of RC hollow columns confined with CFRP. *J. Compos Construct* 2007;11(1). 1090-0268.
21. F.U.A. Shaikh , R. Alishahi. Behaviour of CFRP wrapped RC square columns under eccentric compressive loading. *Structures* 20 (2019) 309–323.
22. A. Saljoughian , D. Mostofinejad. Axial-flexural interaction in square RC columns confined by intermittent CFRP wraps. *Composites Part B* 89 (2016) 85-95.
23. Md A. Hosen, M. Z. Jumaat , A.B.M. Saiful Islam. Side Near Surface Mounted (SNSM) technique for flexural enhancement of RC beams. *Materials & Design* 2015; 83 : 587–597
24. A. Bilotta, F. Ceroni, E. Nigro, M. Pecce. Efficiency of CFRP NSM strips and EBR plates for flexural strengthening of RC beams and loading pattern influence. *Composite Structures* 124 (2015) 163–175.
25. F. Al-Mahmoud, A. Castel, R. François, C. Tourneur. RC beams strengthened with NSM CFRP rods and modeling of peeling-off failure. *Composite Structures* 92 (2010) 1920–1930.
26. H. Pham, R. Al-Mahaidi. Prediction models for debonding failure loads of carbon fiber reinforced polymer retrofitted reinforced concrete beams. *J Compos Construct, ASCE* 2006;10(1):48–59.
27. GJ Xiong, X Jiang, JW Liu, L Chen. A way for preventing tension delamination of concrete cover in midspan of FRP strengthened beams. *Construct Build Mater* 2007;21:402–8.
28. M. A. Zaki , H. A. Rasheed , R. R. Roukerd , M. Raheem. Performance of reinforced concrete T beams strengthened with flexural CFRP sheets and secured using CFRP splay anchors. *Engineering Structures* 210 (2020) 110304.
29. Y. T. Obaidat , W. S. Barham, A. H. Aljarah. New anchorage technique for NSM-CFRP flexural strengthened RC beam using steel clamped end plate. *Construction and Building Materials* 263 (2020) 120246.
30. ACI Committee 440. *Guide For The Design And Construction Of Externally Bonded FRP Systems For Strengthening Concrete Structures*. American Concrete Institute, 2017, Farmington Hills, MI., USA.
31. Yihua Zeng, Xi Chen, Xinghua Li, Gang Wu. Strengthening of RC beams using the combination of EB CFRP sheet, NSM CFRP bar and P-SWRs. *Structural Concrete*. 2021;22:132–145.
32. Hayder Mirdan Abdzaid and Hayder Hussein Kamonna. Flexural Strengthening of Continuous Reinforced Concrete Beams with Near-Surface-Mounted Reinforcement. *Practice Periodical on Structural Design and Construction*, Volume 24 Issue 3 - August 2019
33. L. Li, W. Zheng, Y. Wang. Review of moment redistribution in statically indeterminate RC members. *Engineering Structures* 196 (2019) 109306.
34. RH Scott, RT Whittle. Moment redistribution effects in beams. *Mag Concr Res* 2005;57:9–20.

35. Hesham M.A. Diab, Tarek Abdelaleem, Mohamed M.M. Rashwan. Moment redistribution and flexural performance of RC continuous T-beams strengthened with NSM FRP or steel bars. *Structures* 28 (2020) 1516–1538.
36. Mohammad Abdallah, Firas Al Mahmoud, M. Idriss Tabet-Derraz, Abdelouahab Khelil, Julien Mercier. Experimental and numerical investigation on the effectiveness of NSM and side-NSM CFRP bars for strengthening continuous two-span RC beams. *Journal of Building Engineering* 41 (2021) 102723
37. CNR-DT 200 R1/2013, Guide for the design and construction of externally bonded FRP systems for strengthening existing structures, Rome, Italy: National Research Council; 2013.
38. FIB Bulletin 14. Externally Bonded FRP Reinforcement for RC Structures. International Federation for Structural Concrete, Zürich, Switzerland, 2001.
39. ACI. Building code requirements for structural concrete and commentary. American Concrete Institute, ACI 318-14, Farmington Hills, MI., September 2014.
40. BS EN 1992-1-1:2004. Eurocode 2: Design of concrete structures - Part 1–1: General rules and rules for buildings. London, UK: British Standards Institution; 2004.
41. AS 3600-2009. Concrete structures. Sydney, Australia: Australia Standards; 2009.
42. M. A. Aiello, L. Valente, and A. Rizzo. Moment Redistribution In Continuous Reinforced Concrete Beams Strengthened With Carbon-Fiber-Reinforced Polymer Laminates. *Mechanics of Composite Materials*, Vol. 43, No. 5, 2007.
43. R. Feng, Y. Liu, J-H. Zhu, F. Xing. Flexural behaviour of C-FRCM strengthened corroded RC continuous beams. *Composite Structures* 245 (2020) 112200.
44. D.J. Oehlers, G. Ju, I.S.T. Liu, R. Seracino. Moment redistribution in continuous plated RC flexural members. Part 1: neutral axis depth approach and tests. *Engineering Structures* 26 (2004) 2197–2207.
45. M. Cohn. Continuity in prestressed concrete partial prestressing from theory to practice, vol I, Survey Reports, NATO ASI Series Boston, Mass: Martinus Nijhoff Publishers. 1986. p. 189–256.

### ***Highlights***

- The side bonding technique is a convenient alternative to the conventional EB and NSM techniques for strengthening continuous RC beams.
- Increasing the carbon fiber weight per unit area was found to be effective in improving the strength capacity of continuous RC beams and it may ~~use~~ serve as an alternative to multiple sheet layers.
- The majority of the moment redistribution of EB-CFRP beams occurred in the stage between the concrete cracking and the first steel yielding.
- The current design codes can accurately predict the ultimate strength of continuous RC beams strengthened with one CFRP layer, but not with multiple layers.

- The test results confirm that the NSM system is more efficient than the EB for the strengthening of continuous RC beams. ~~allow confirming the higher efficiency of the NSM system in comparison to the EB one for strengthening continuous RC beams.~~